

ISTANBUL TECHNICAL UNIVERSITY ★ INFORMATICS INSTITUTE

**DESIGN OF MICROSTRIP PATCH ANTENNAS
FOR 5G MOBILE COMMUNICATION SYSTEMS**



M.Sc. THESIS

Ferda Cansu GÜL

Department of Applied Informatics

Information and Communication Engineering Programme

DECEMBER 2019

ISTANBUL TECHNICAL UNIVERSITY ★ INFORMATICS INSTITUTE

**DESIGN OF MICROSTRIP PATCH ANTENNAS
FOR 5G MOBILE COMMUNICATION SYSTEMS**

M.Sc. THESIS

**Ferda Cansu GÜL
(708161020)**

Department of Applied Informatics

Information and Communication Engineering Programme

Thesis Advisor: Asst. Prof. Dr. Sebahattin EKER

DECEMBER 2019

İSTANBUL TEKNİK ÜNİVERSİTESİ ★ BİLİŞİM ENSTİTÜSÜ

**MİKROSTRİP ANTENLERİN
5G MOBİL İLETİŞİM SİSTEMLERİ İÇİN TASARLANMASI**

YÜKSEK LİSANS TEZİ

**Ferda Cansu GÜL
(708161020)**

Bilişim Uygulamaları Anabilim Dalı

Bilgi ve Haberleşme Mühendisliği

Tez Danışmanı: Dr. Öğr. Üyesi Sebahattin EKER

ARALIK 2019

Ferda Cansu GÜL, a M.Sc. student of ITU Informatics Institute 708161020, successfully defended the thesis entitled “DESIGN OF MICROSTRIP PATCH ANTENNAS FOR 5G MOBILE COMMUNICATION SYSTEMS” which she prepared after fulfilling the requirements specified in the associated legislations, before the jury whose signatures are below.

Thesis Advisor : **Asst. Prof. Dr. Sebahattin EKER**
İstanbul Technical University

Jury Members : **Prof. Dr. Orhan İÇELLİ**
Yıldız Technical University

Doç. Dr. Vasil Tabatadze
İstanbul Technical University

Date of Submission : 15 November 2019

Date of Defense : 11 December 2019





To my family,



FOREWORD

I would like to thank my supervisor Asst. Prof. Dr. Sebahattin EKER, for his valuable support and encouragement. He always guided me and motivated me not only during my studies but also in my academic footsteps.

I would like to thank ITU BAP, support this thesis under the project with the ID number 41977. For the reason that this work is supported in part by Istanbul Technical University (ITU) Vodafone Future Lab under Project ITUVF20180901P10, I also would like to thank ITU Vodafone Future LAB. I would like to thank TÜBİTAK due to their support for my thesis with a scholarship under the name 2210-C. I would like to thank Alev KESKİN from ITU MEAM Laboratory due to his helping during the fabrication process of the antennas. I also would like to thank TÜBİTAK ATAM for their help during the measurements of the antennas.

I also would like to present my gratitude to Prof. Dr. Ertuğrul KARAÇUHA. He always shares his experiences and support without hesitation.

I would like to thank my friend and also my colleague Kamil KARAÇUHA for his directions and suggestions for my study. He is always eager to share what he knows in the subject. I am lucky to have the chance to work with him.

I want to thank my spouse and my love Ahmet Kürşad GÜL for his support in every step of my life. Moreover, he always contributes my works in theoretical and technical levels. His point of view always guides me and protects me.

As a final word, I want to thank my family for their relieving and strengthening me in every decision I made. I would not feel whole without them.

December 2019

Ferda Cansu GÜL
(Physics Engineer)

TABLE OF CONTENTS

	<u>Page</u>
FOREWORD	ix
ABBREVIATIONS	xiii
LIST OF TABLE	xv
LIST OF FIGURE	xvii
SUMMARY	xix
ÖZET	xxi
1. INTRODUCTION	1
1.1 5G Antennas and Spectrum Analyze.....	1
1.2 Organization of Thesis	2
2. ANTENNA THEORY	5
2.1 Antenna Radiation Principles.....	5
2.1.1 Maxwell's equations	6
2.2 Radiation Basics	7
2.2.1 Radiated fields of an antenna	9
2.3 Basic Antenna Parameters.....	11
2.3.1 Radiation pattern	11
2.3.2 Beamwidth	13
2.3.3 Directivity	14
2.3.4 Gain.....	15
2.3.5 Input impedance, scattering parameters and bandwidth	16
3. ANTENNAS	19
3.1 Microstrip Antennas	19
3.1.1 Rectangular patch antennas.....	21
3.1.2 Circular patch antennas	22
3.1.3 Dipole and loop antennas	23
3.2 Reflector Antennas	25
3.3 Array Antennas.....	26
4. ANTENNA DESIGN	29
4.1 Feeding Mechanism	29
4.1.1 Microstrip feeding.....	29

4.1.2	Probe feeding.....	30
4.1.3	Proximity feeding.....	30
4.1.4	Aperture coupling feeding.....	31
4.2	Simulation Techniques and Tools	32
4.2.1	HFSS (High Frequency Simulation Software).....	32
4.2.2	CST microwave studio program	33
5.	DUAL BAND QUASI-YAGI ANTENNA.....	35
5.1	Single Element Design	35
5.1.1	Simulation and experimental results	37
5.2	Two Element Array Design	38
5.3	Four Element Design	41
5.3.1	Simulation and experimental results	42
5.4	Virtual Array Design	43
5.4.1	Unit cell antenna.....	43
5.4.2	Two element array antenna	46
6.	CIRCULAR DIPOLE ANTENNA	51
6.1	Single Element Design	51
6.1.1	Simulation and experimental results	52
6.2	Two Element Array Design	54
6.2.1	Simulation and experimental results	55
7.	K BAND ANTENNA DESIGN	57
7.1	Single Element Design	57
7.1.1	Simulation and experimental results	58
8.	CONCLUSION AND FUTURE WORK	61
	REFERENCES	63
	CURRICULUM VITAE	67

ABBREVIATIONS

IoT	: Internet of Things
CST	: Computational Simulation Tool
HFSS	: High Frequency Simulation Software
CPW	: Coplanar waveguide
dB	: Decibel
PEC	: Perfectly Electrical Conductor





LIST OF TABLE

	<u>Page</u>
Table 3.1: Dielectric Substrates Properties.	20
Table 5.1: Antenna Parameters.	37
Table 5.2: Peak Values for S_{11}	38
Table 5.3: Parametric Results vs Distance	40
Table 5.4: Parameter Values	42
Table 6.1: Design Parameters.	52
Table 7.1: Design Parameters.	58



LIST OF FIGURE

	<u>Page</u>
Figure 2.1: Radiation Basics a) Dipole Radiation Formation b) Radiated Field	7
Figure 2.2: Ideal Dipole Configuration.....	8
Figure 2.3: Radiation Representation for Ideal Dipole a) E and H Fields Vectors b) E-plane Radiation Pattern Polar Plot c) H-plane Radiation Pattern Polar Plot c) Radiation Pattern in 3D.....	9
Figure 2.4: Field Regions.....	10
Figure 2.5: Radiation Characteristic with Respect to the Distance.....	10
Figure 2.6: The Spherical Coordinate System Configuration for an Antenna.....	12
Figure 2.7: Solid Angle Definiton.....	13
Figure 2.8: The Beam Classification Graph for Radiation Pattern of an Antenna ...	14
Figure 2.9: Omnidirectional Pattern.....	15
Figure 2.10: Two Port Network	16
Figure 3.1: Microstrip Antenna Basics	19
Figure 3.2: Different Types of Patch Shapes	20
Figure 3.3: Rectangular Patch Antenna Configuration.....	21
Figure 3.4: Circular Patch Antenna.....	22
Figure 3.5: Electric Field Orientation of an Infinitesimal Dipole.....	23
Figure 3.6: Loop Antenna	24
Figure 3.7: Image Theory Representation for E-Fields.	25
Figure 3.8: Array Configuration a) Two Dipole b) at Far-Field.....	26
Figure 4.1: Microstrip Feeding Line	30
Figure 4.2: Probe Feeding	30
Figure 4.3: Proximity Feeding a) from Top, b) from Side View.....	31
Figure 4.4: Aperture Coupling Method	31
Figure 4.6: CST Mesh Configuration	33
Figure 5.1: Unit Cell Quasi-Yagi Antenna.	36
Figure 5.2: Fabricated Unit Cell Antenna.....	36
Figure 5.3: 2D and 3D Simulated Radiation Pattern for Unit Cell (a) and (b) for 2.3 Hz; (c) and (d) for 3.5 GHz.....	37
Figure 5.4: S_{11} vs Frequency Graph for Simulated and Experimental Data.....	38
Figure 5.5: 1x2 Array Antenna Design.....	39
Figure 5.6: Fabricated Antenna.....	39
Figure 5.7: 3D Radiation Pattern of Two Element Array.....	40
Figure 5.8: Current Density of Two Element Array (a) 2.3 GHz and (b) 3.5 GHz..	40
Figure 5.9: S_{11} and S_{21} Values.	41
Figure 5.10: Four Element Antenna Design.	41
Figure 5.11: Fabricated Antenna.....	42

Figure 5.12: S_{11} and S_{21} Values.....	42
Figure 5.13: 3D Radiation Pattern (a) 2.3 GHz and (b) 3.5 GHz.	43
Figure 5.14: Fabricated Unit Cell Antenna.	43
Figure 5.15: Anechoic Chamber and Far-Field Measurement for Fabricated Antenna.	44
Figure 5.16: 3D Radiation Pattern (a) 2.3 GHz and (b) 3.5 GHz.	44
Figure 5.17: Simulated 2D Radiation Pattern for Different “L” Values (a),(b) 2.3 GHz and 3.5 GHz in E-plane; (c),(d) 2.3 GHz and 3.5 GHz in H-plane.	45
Figure 5.18: Simulated 2D Radiation Pattern for Different “h” Values (a),(b) 2.3 GHz and 3.5 GHz in E-plane; (c),(d) 2.3 GHz and 3.5 GHz in H-plane.	45
Figure 5.19: Experimental Results of the Radiation Pattern for a),b) E and H planes without Reflector c),d) E and H-plane with Reflector.	46
Figure 5.20: S_{11} Values.	46
Figure 5.21: Simulated 3D Pattern and Antenna Configuration a) 2.3 GHz and b) 3.5 GHz.	47
Figure 5.22: “L” Length of the Copper Reflector Plate (a) 2.3 GHz (b) 3.5 GHz for E-plane ($\Phi=0^\circ$) ; (c) 2.3 GHz 5 GHz for H-plane ($\theta=90^\circ$).....	47
Figure 5.23: “h” Parametrical Result in 2D Radiation Pattern (a) 2.3 GHz and (b) 3.5 GHz at the E-plane ($\Phi =90^\circ$) and (c) 2.3 GHz and (d) 3.5 GHz at the H-plane ($\theta=0$) for L= 75mm; h=5mm; 20mm; 40mm.	48
Figure 5.24: The Current Density with Reflector Plate (a) 2.3 GHz (b) 3.5 GHz. ...	48
Figure 5.25: Fabricated Antenna.....	49
Figure 5.26: S_{11} and S_{21} Graph.....	49
Figure 6.1: Design Configurations of the Antenna a) Front b) Back Side.....	52
Figure 6.2: Fabricated Antennas a),b) Referenced Geometry Ant1 c),d) Modified Geometry Ant2.	52
Figure 6.3: S_{11} Result for Reference and Modified Antenna.....	53
Figure 6.4: Radiation Pattern Measurement in Far-Field.....	53
Figure 6.5: Antenna Configuration in Simulation Tool.	54
Figure 6.6: 2D Radiation Pattern a),b) Simulated Results; c),d) Experimental Results.	54
Figure 6.7: Antenna Configuration.	55
Figure 6.8: Fabricated Antenna.....	55
Figure 6.9: S_{11} and S_{21} Parameters.....	56
Figure 6.10: 2D Radiation Patterns a) in E-field b) in H-field.....	56
Figure 7.1: Antenna Design a) Antenna without Reflected Back b) with Reflected Back.....	57
Figure 7.2: Antenna Design Simulation.....	58
Figure 7.3: Gain Results a) 26 GHz, b) 28 GHz, c) 30 GHz.	59
Figure 7.4: Gain Results Reflected Element a) 26 GHz, b) 28 GHz, c) 30 GHz.....	59
Figure 7.5: Antenna Design with SMA Connector Simulation.	59
Figure 7.6: Far-Field Gain Results a) 26 GHz, b) 28 GHz, c) 30 GHz.....	60
Figure 7.7: Simulated S_{11} Parameters.	60

DESIGN OF VARIOUS TYPES MICROSTRIP PATCH ANTENNAS FOR 5G MOBILE COMMUNICATION SYSTEMS

SUMMARY

The number of connected people and devices getting rise as a result of IoT adoption causes an increased demand for mobile communication systems. However, the spectrum is limited and the problem should be solved by using the spectrum efficiently. Therefore, shifting the bands we use today to the high-frequency range brings up the usage of the millimeter-wave spectrum, for the reason that high data capacity and low latency properties of the spectrum.

In the thesis, three different antenna designed has been proposed. The antennas firstly designed and simulated as a unit cell. Firstly, the Quasi-Yagi antenna with the dual-band feature has been presented as a reference design. The antenna operates in two different bands with two different radiation characteristics. In 2.4 GHz Wi-Fi band, the antenna has an omnidirectional pattern and for 3.5 GHz the radiation pattern is directive. In case of having more directive and increased gain antenna, the unit cell has antenna has been designed as an array with four-element and two inputs. By doing this, the gain is increased and the design is planned to be used for beamforming applications. The antenna designs have been fabricated and its matching properties and radiation patterns have been performed experimentally in an anechoic chamber. The simulated and experimental results have been represented in the corresponding chapters.

The last design has been modeled to operate at the K_a band which covers the 27-35 GHz spectrum. The antenna has been studied by adding the geometry SMA component due to observing its effects. As the final step, a reflector element is added to the structure to eliminate the sidelobes of the radiation. The millimeter-wave antenna design will be studied as an array design for the beamforming applications as future work.

As the next step, the optimization of matching parameters of four-element design will be enhanced. The sidelobe reduction of the circular dipole design will be studied by adopting the design an vertical array system. K_a band unit cell antenna design will be optimized and fabricated. The prototypes of the antennas will be measured experimentally. The experimental results of the studied antennas will be presented.



FARKI TİP MİKROSTRİP ANTENLERİN 5G MOBİL İLETİŞİM SİSTEMLERİ İÇİN TASARLANMASI

ÖZET

IoT'ye adapte olma sürecinde, internete bağlı insanların ve cihazların sayısındaki artış sebebiyle mobil iletişim sistemlerine talep yoğun bir şekilde artmaktadır. Bununla beraber, spektrumun sınırlı oluşu nedeniyle bu talep ancak elimizdeki spektrumun verimli kullanımıyla çözülebilir. Bu yüzden, bugün kullandığımız spektrumun yüksek frekanslara kayışı, yüksek data kapasitesi ve düşük gecikme özellikleri sebebiyle milimetrik dalga spektrumunu kullanımı beraberinde getirmektedir.

Bu tezde, üç farklı anten dizaynı önerilmektedir. Tüm tasarımlar önce birim hücre olarak tasarlanmış ve ardından sıralı olarak düzenlenmişlerdir. Tezde önerilen çift bantta çalışan anten ile hem Wi-Fi sistemler için hem de 5G'ye geçiş fazında ara bant olarak kullanılması planlanan 3.5 GHz bandını kapsamıyla mobil iletişim sistemleri için katkı sağlanması amaçlanmıştır. Diğer birim hücre tasarımı için çembersel dipol anten tasarımı seçilmiştir. Bu anten de yine 3.5 GHz bandını kapsamının yanı sıra, 5.8 GHz WiFi bandında da çalışan geniş bantlı bir tasarımdır. Bu birim hücre tasarımlarını iki elemanlı iki girişli tasarıma dönüştürerek çoklu girişli sıralı anten dizaynları gerçekleştirilmiştir. Bu anten tasarımlarıyla IoT sistemlerde ışınımın akıllı kontrolü uygulamalarında yer bulunması amaçlanmıştır. Çoklu girişli sistemlerin mobil teknolojilerde bir çok alanda kullanımı vardır. Girişlere faz farkı uygulayarak ışınımın istenilen açılarda döndürülmesi, bu çalışmanın devamı olarak gerçekleştirilmesi planlanan çalışmalardandır.

5G'nin en önemli aşamalarından biri olarak, milimetre-dalga spektrumu için uygun komponent tasarımlarının gerçekleştirilmesi söylenebilir. Bu doğrultuda tezde K_a bantta çalışan bir birim hücre tasarımına yer verilmiştir. Milimetre-dalga boyu için antenlerin boyutu oldukça küçülmektedir. Ayrıca, bu tasarımların üretiminden ölçüm sürecine kadar günümüz temel teknolojisinde kullandığımız cihazlardan daha hassas sistemler gerekmektedir. Bunun en büyük nedeni ise yüksek frekansta çalışan antenin sahip olduğu elektromanyetik dalga boyunun çevresel etkilerden dolayı ortamda gücünü hızla kaybetmesidir.

İlk olarak, çift bantta çalışan Quasi-Yagi anten tipi referans dizayn olarak ele alınmıştır. Anten, 2.4 Wi-Fi bandında her yönlü ışınım gösterirken, 3.5 GHz 5G mobil iletişim bandında yönlü ışınım göstermektedir. Sıralı anten tasarımları antenin yönlülük ve kazamç özelliklerini iyileştirirken, saçılma parametresi değerlerini de korumak ve iyileştirmek üzere tasarlanmıştır. Bu tasarım için kazanç düşük frekans için 1.3 dB, yüksek frekans için 5.2 dB olarak belirlenmiştir. Eşleşme değerleri ise her iki frekans için -15 dB altındadır. Birinci sıralı anten tasarımında iki hücreli iki girişli tasarım gerçekleştirilmiştir. Burada kazanç değeri 4.9 dB ve 8 dB olarak düşük ve yüksek frekans bantları için belirlenmiştir. Saçılma parametresi yani eşleşme değerleri

de -15 dB değerinin altındadır. İkili girişli tasarımlarda her iki girişin birbiriyle olan etkilişimini gösteren S_{21} değerleri de çalışılmıştır. Bu değer -20 dB ve üzerinde olması beklenirken, çalışılan tasarımda bu gereklilik de sağlanmıştır. Quasi-Yagi anten tipi için uygulanan dört elemanlı tasarım için iki giriş konumlandırılmıştır ve bu girişler temel bir güç bölücü ile birleştirilmiştir. Bu tasarımda da, iki rezonans frekansında 6.2 dB ve 8.3 dB kazanç değerleri elde edilmiş olup buna rağmen güç bölücü yalnızca 3.5 GHz bandı için çalışmaktadır.

Birim hücre tasarımı ve iki hücreli sıralı anten tasarımları reflektör düzlem üzerinde simüle edilmiş ve bu sayede kazanç parametreleri iyileştirilmiştir. Birim hücre tasarımı için kazanç 2.3 GHz frekansında 1.3 dB değerinden 6.52 dB değerine; 3.5 GHz frekansında 5.8 dB değerinden 8.3 dB değerine çıkarılmıştır. Sonrasında, iki eleman içeren tasarımın reflektör düzlem üzerinde simülasyon çalışmaları yapılmıştır. Bu tasarımda da kazanç sırasıyla 2.3 GHz ve 3.5 GHz için, 4.9 dB değerinden 10.1 dB değerine, 8 dB değerinden 13.2 dB değerine çıkarılmıştır.

Bir sonraki adımda tasarlanmış olan çoklu girişli Quasi-Yagi antenlerden dört hücreli antenin saçılma parametrelerinin iyileştirilmesi ve optimize edilmiş bir güç bölücü ile tasarlanması öngörülmektedir. Optimizasyonu başarılı olan iki hücreli anten ve çoklu girişli anten tasarımları ile akıllı anten denemeleri yapılması planlanmaktadır.

Çembersel dipol anten tasarımı da referans antenin geniş bantlı operasyon bandının yüksek frekansa kaydırılmasıyla hem 3.5 GHz hem de 5.8 GHz bandın kapsamı sağlanmıştır. Bu tasarımda bahsedilen frekans değerleri için kazanç değerleri sırasıyla 5 dB ve 3.7 dB olarak gösterilmiştir. Tasarımın iki eleman ve iki giriş içeren formdaki simülasyon sonuçlarında, bahsedilen frekans değerleri için kazanç değerleri 6.0 dB ve 6.3 dB olarak belirlenmiştir.

FR-4 malzemesi ile HFSS kullanılarak simülasyonu yapılmış Quasi-Yagi ve çembersel dipol antenlerinin üretimi de gerçekleştirilmiş ve değerler deneysel olarak ölçülmüştür. Üretim safhasında LPKF üretim tezgahı kullanılmıştır. Ölçümler için ise saçılma parametreleri Network Analyzer ile ölçülmüş olup, uzak alan radyasyon diyagramları yankısız odada ölçülmüş ve belirlenmiştir. Bu sonuçlar tezde ilgili bölümlerde sunulmuştur. Işıma diyagramlarında simülasyon sonuçları ile deneysel olarak ölçülen uzak alan ışımaya diyagramları ana loblar açısından uyum içerisindedir. Bununla beraber arka ve yan loblarda bozulmuş bir grafik söz konusudur. Deneysel ölçümler, bir çok etkenden dolayı radyasyon diyagramlarında bozulmalara yol açabilmektedir. Ana diyagramlardaki uyum üretilmiş antenin simülasyon sonuçlarını destekler niteliktedir.

Bu çalışmanın devamı olarak, sıralı çembersel dipol antenin dikey düzlemde de sıralanmış bir tasarımının dizayn edilmesi planlanmaktadır. Bu şekilde optimize edilecek antenin ışımaya diyagramında meydana gelen yan lobları azaltması beklenmektedir. Birim hücre antenle yine çoklu girişli ve daha fazla sayıda birim hücre ile tasarlanmış sıralı anten tasarımları çalışılacaktır.

Son olarak gerçekleştirilen tasarımda anten K_a bandında çalışmakta olup, bu bant 27-35 GHz frekans aralığına karşılık gelmektedir. Yüksek frekans antenlerin çevre faktörlerden kolayca etkilenmesi sebebiyle anten SMA konektörü de modellenerek simüle edilmiş ve kıyaslama sonuçları ilgili bölümde sunulmuştur. Bir reflektör elementin tasarıma eklenmesiyle radyasyon yan loblarının elimine edilmesine çalışılmış ve kazanç ve yönlülüğün iyileştirilmesi hedeflenmiştir. Simülasyon

çalışmaları bu anten için CST programı kullanılarak gerçekleştirilmiştir. Simulasyon sonuç ve grafikleri ilgili bölümde sunulmuş ve analiz edilmiştir.

Gelecek çalışma olarak öncelikle K_a bandı birim hücre antenin özelliklerinin iyileştirilmesi amaçlanmaktadır. Birim hücrede istenilen frekans bandında verimli şekilde çalışan antenin çoklu elemanlı sıralı anten tasarımına uyarlanması için gerekli simülasyon çalışmaları gerçekleştirilecektir. Simüle edilen antenin üretimi ve deneysel olarak ölçülebilmesi için gereken substratlar temin edilecektir.





1. INTRODUCTION

In a communication system, the technology of the antenna component has a very crucial place defining the quality of the system. Besides that, 5G has started to define recent demands that are arisen with the IoT. Mobile communications systems take a very important place in IoT, due to the increased number of wireless network users who remain being connected. The IoT environment is being built with challenges that bring about that the 5G uses are an urgency. Increasing the coverage of mobile broadband, low latency and increasing the capacity can be counted as main challenges that expected to be enhanced by using the 5G spectrum. The component technology of mobile communication systems should be evolved into the 5G requirements in this sense. The antenna designs studied in this thesis, has been chosen to cover the bands; 2.4, 5.8 GHz WiFi bands, 3.5 GHz and 28 GHz mobile communication bands which are defined new 5G spectrums[1-3].

The antenna geometries have been studied by considering the feasibility of the fabrication process. Three base antenna geometries have been involved in the thesis; the Quasi-Yagi, circular dipole antenna and triangular patch antenna with a coplanar waveguide fed. The Quasi-Yagi antenna has been transformed into two-element geometry and its gain properties have been increased by using reflectors for both unit cell and two-element geometry. Four element Quasi-Yagi antenna has been also studied to enhance radiation characteristics. Circular dipole antenna geometry has been studied as a unit cell design and after that, it also adopted to two-element array design. The final design has been presented in the thesis is the triangular patch with CPW (Coplanar waveguide) operates at the K band and because the design has very small geometry, it is a very good candidate for array design.

1.1 5G Antennas and Spectrum Analyze

As a result of the IoT and 5G, to meet the expectations there must be organized the new solutions for remote and smart controlling systems that require high data transfer by using the mobile communication systems. Connected and smart houses, shopping

centers, parks, workplaces; factories or offices and public areas are supposed to be assisted by innovative software and hardware systems. However, due to having a limited spectrum for each application, data traffic should be managed effectively by applying practical solutions. The local networks and unlicensed bands in the spectrum are having attention as a result of the necessity of efficiency [4-6].

The Quasi-Yagi antenna has been studied in thesis due to design have dual-band feature and its structure is low profile, low cost and easy to manufacture advantages. The dual-band property is very useful because of providing two spectrum usage for different applications at the same time. By adding new geometries, the Quasi-Yagi antenna designs have been improved to adapt to new technological requirements. The applications where Quasi-Yagi antennas have places can be listed as radar applications, WiFi, RF harvesting, etc. [7-12].

Wideband and ultrawideband antennas can be used for their high data capability properties and these antennas can be applied to radar application and wideband communication systems. Circular patch antennas may have wideband characteristics unlikely the other resonance type antennas. Moreover, they are ease to fabricate and can be modified with slots, number of inputs or they can be designed in array geometries [13-17].

By the 5G, the millimeter-wave spectrum has been started to be studied for the reason that its large bandwidth provides high capacity with respect to the microwave spectrum. In this spectrum, the millimeter-wave range is started with the 30 GHz. However, the standards define the K_a band, where it covers 26.5 GHz- 40 GHz, which is a new mobile band communication band. Specifically for 28 GHz, many antenna designs have been performing because of the millimeter waves not only have benefits but also challenges due to its high attenuation loss. Besides that, millimeter-wave antennas are convenient structures to use in array designs. In literature, different antenna structures like coplanar waveguide fed designs and array designs with a variety of geometry have been published. [18-22].

1.2 Organization of Thesis

The study of the thesis has been realized for the purpose that designing unit cell antennas before the transition to array designs. The 2nd, 3rd, 4th chapters contain the

theoretical background for designing an antenna. In the second chapter, antenna theory has been summarized around the center of types used in the thesis. The basic antenna structure has been analyzed by using Maxwell's equations and far-field regions are defined for small and large antennas. In the third chapter, the antenna types have been represented by considering the designs that have been studied in the thesis. In the fourth chapter, the simulation software programs have been presented and the feeding technics for microstrip antennas have been explained.

Study of designing, fabricating and measuring the specified antenna structures have been explained in the 5th, 6th, and 7th chapters. Chapter five included the Quasi-Yagi antenna design with its variations. After achieving the desired parameters for the unit cell, the designs have been adopted to two and four cells array. The gain and directivity properties have been enhanced by using a reflector that provides a virtual array for single element dual-band Quasi-Yagi antenna design and its two-element design. In the 6th chapter, a wideband circular geometry study has been presented. The unit cell is modified from reference geometry and then it has been converted to two cell two input array design. In the last chapter, the K_a band antenna has been studied at the simulation level. The antenna has a novel geometry and fed by coplanar waveguide structure. Due to the millimeter-wave antennas are vulnerable for environmental impact, the simulations are also done by adding the SMA connector the geometry.



2. ANTENNA THEORY

Electrical signals can travel via transmission lines or through space by using antennas at destination points. Electromagnetic waves are carried via transmission lines which often use a balanced system of conductors or a metallic coverage to confine the energy. However, the scenario mostly asks for transmitting or receive the energy from a very long distance that requires very long transmission lines. Antennas are reciprocal devices, the definition is given by IEEE “that part of a transmitting or receiving system that is designed to radiate or to receive electromagnetic waves” [23]. Moreover, antennas are capable to be optimized for shaping the radiation beam in the specified direction. Thus, the antenna is not only transmitting or receiving the signal but also reshape it. Antennas are used inevitably in many numbers of applications where wireless communication takes place such as; medical applications, space communication, military and radar applications. Application area determines the radiation characteristics which can be created by applying different geometries to antenna. Some of those antennas are named as hellical, loop, aperture, patch antennas. Antennas performance have very critical effects on overall system and it defines the quality of service in a sense.

2.1 Antenna Radiation Principles

Electromagnetic waves propagate in a medium as a result of a disturbance of electromagnetic field. Time-varying current causes radiation under specific circumstances that are like the path is bent, curved, discontinuous, terminated. One of the most important features of antennas has is that the power does not corrupt by the distance. As long as the source maintains and the wave does not encounter an obstacle, electromagnetics wave travels continuously. Analyzing and designing antennas is a problem that requires the solution based on Maxwell’s equation. The basic point to start to construct the solution is defining the radiation which is occurred due to a single accelerating charge and applying Maxwell's equations to configuration.

2.1.1 Maxwell's equations

Maxwell's equations are needed to be constructed on spherical coordinates due to the reason that the radiation field of the antenna is observed in all directions. Moreover, the expression of fields is in vector form because the direction of fields explains important features that can be analyzed under the subtitles, which are polarization or directivity. The fundamental electromagnetic equations in time domain are expressed between Equation 2.1-5 where \mathbf{E} and \mathbf{H} are the electric and magnetic field in time domain, respectively. φ_T and ρ_T define the sources.

The equations can be reduced simplyfy form by using the definition of phasor fields as in Eq 2.6 and field equations are indicated in Eq 2.7-10.

$$\mathbf{E} = \text{Re}(\mathbf{E}e^{j\omega t}), \mathbf{H} = \text{Re}(\mathbf{H}e^{j\omega t}) \quad (2.6)$$

$$\nabla \times \mathbf{E} = -j\omega\mathbf{B} \quad (2.7)$$

$$\nabla \times \mathbf{H} = j\omega\mathbf{D} + \mathbf{J}_T \quad (2.8)$$

$$\nabla \cdot \mathbf{D} = \rho_T \quad (2.9)$$

$$\nabla \cdot \mathbf{B} = 0 \quad (2.10)$$

The complex power which flows out through closed surface is described as in Eq 2.11.

$$P_f = \frac{1}{2} \oint\oint_s \mathbf{E} \times \mathbf{H}^* \cdot d\mathbf{s} \quad (2.11)$$

The term inside the integrand is named as Poynting vector which is written as in Equation 2.12.

$$\mathbf{S} = \frac{1}{2} \mathbf{E} \times \mathbf{H}^* \quad (2.12)$$

The real power is defined as real part of the power;

$$P = \frac{1}{2} \text{Re} \int\int \mathbf{E} \times \mathbf{H}^* \cdot d\mathbf{s} \quad (2.13)$$

The main concern in the antenna problems to obtain the electrical and magnetic fields which are created by current distribution \mathbf{J} . Thus, from the point knowing the current distribution, the fields can be calculate by using Equation 2.14;

$$\mathbf{A} = \iiint_{\vartheta} \mu \mathbf{J} \frac{e^{-j\beta R}}{4\pi R} d\vartheta' \quad (2.14)$$

where the \mathbf{A} is the magnetic vector potential and the magnetic field is the curl of the \mathbf{A} , which is indicated as;

$$\mathbf{H} = \frac{1}{\mu} \nabla \times \mathbf{A} \quad (2.15)$$

β is defined as the phase constant of propagating wave which is a measure of phase shifts per distance and it can be defined by using parameters; “f” frequency, “w” radian frequency, “ ϵ ” permittivity, “ μ ” permeability, “ λ ” wavelength and “c” speed of light in vacuum, between Equation 2.16-17.

$$\beta = w\sqrt{\mu\epsilon} \quad (2.16)$$

$$\beta = \frac{2\pi}{\lambda} = \frac{2\pi f}{c} = \frac{w}{c} \quad (2.17)$$

The speed of light can be calculated by using the expression,;

$$c = \frac{1}{\sqrt{\epsilon_0\mu_0}}, \text{ which is equal to } 3 \times 10^8 \text{ m/s}$$

2.2 Radiation Basics

As mentioned above section, the electromagnetic wave propagates as a result of transferring the energy in the field by disturbing the existing field. The radiated field preserves its energy and it is not incurred losses as it goes away from the source as long as the source is active. In Figure 2.1, the radiated field from dipole is presented. The basic principle of radiated field calculations relies on the ideal dipole configuration which is indicated in Figure 2.2.

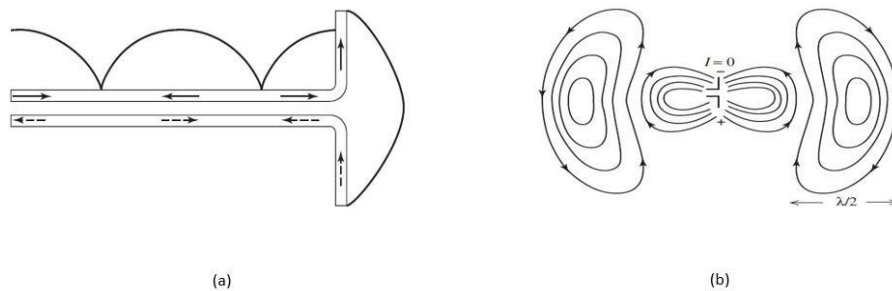


Figure 2.1: Radiation Basics a) Dipole Radiation Formation b) Radiated Field [23].

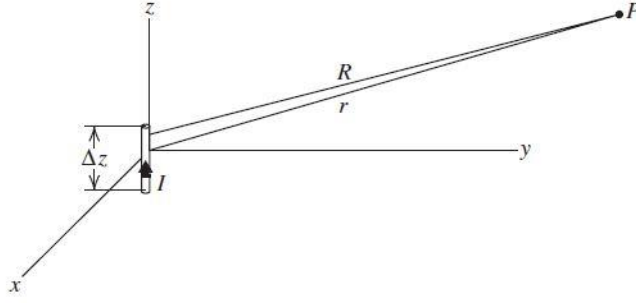


Figure 2.2: Ideal Dipole Configuration [24].

The calculation the field which is occurred due to the ideal dipole can be explained by using the Equations 2.18-2.22 where Equation 2.22 defines the transformation between the cartesian coordinates to the spherical coordinates. The electrical and magnetic fields are concluded as in Equation 2.23 and 2.24.

$$J = I \delta(x') \delta(y') \hat{z} \text{ for } \frac{\Delta z}{2} < z' < \frac{\Delta z}{2} \quad (2.18)$$

$$\mathbf{A} = \hat{z} \mu I \int_{-\infty}^{\infty} \delta(x') dx' \int_{-\infty}^{\infty} \delta(y') dy' \int_{-\frac{\Delta z}{2}}^{\frac{\Delta z}{2}} \frac{e^{-j\beta R}}{4\pi R} dz'$$

$$\mathbf{A} = \frac{\mu I}{4\pi r} e^{-j\beta r} \Delta z \hat{z}$$

$$\mathbf{H} = \frac{1}{\mu} \nabla \times \mathbf{A}$$

$$\hat{r} \times \hat{z} = \hat{r} \times (\hat{r} \cos\theta - \hat{\theta} \sin\theta) = -\hat{\Phi} \sin(\theta) \quad (2.22)$$

$$\mathbf{H} = \frac{I \Delta z}{4\pi} \beta \left[1 + \frac{1}{j\beta r} \right] \frac{e^{-j\beta r}}{r} \sin(\theta) \hat{\Phi} \quad (2.23)$$

$$\begin{aligned} \mathbf{E} &= \frac{I \Delta z}{4\pi} j\omega\mu \left[1 + \frac{1}{j\beta r} - \frac{1}{\beta r^2} \right] \frac{e^{-j\beta r}}{r} \sin(\theta) \hat{\theta} \\ &+ \frac{I \Delta z}{2\pi} \eta \left[\frac{1}{r} - j \frac{1}{\beta r^2} \right] \frac{e^{-j\beta r}}{r} \cos\theta \hat{r} \end{aligned} \quad (2.24)$$

For far-field, the βr term gets larger and it causes that the terms contain $\frac{1}{r^3}$ and $\frac{1}{r^2}$ do not remain in far-field equations which are written in Equations 2.25-2.26.

$$\mathbf{H} = \frac{I \Delta z}{4\pi} j\beta \frac{e^{-j\beta r}}{r} \sin(\theta) \hat{\Phi} \quad (2.25)$$

$$\mathbf{E} = \frac{I \Delta z}{4\pi} j\beta \frac{e^{-j\beta r}}{r} \sin(\theta) \hat{\theta} \quad (2.26)$$

In Equation 2.27, the intrinsic impedance is presented which is η and for the free space $\eta_0 = 376.7\Omega \approx 120 \pi\Omega$. Although this property belongs to plane waves, when the antenna at far distance, this property applies to the relationship between the E and H fields.

$$\frac{E_\theta}{H_\phi} = \frac{w\mu}{\beta} = \frac{w\mu}{w\sqrt{\mu\varepsilon}} = \sqrt{\frac{\mu}{\varepsilon}} = \eta \quad (2.27)$$

While analyzing the properties of an antenna, radiation pattern is studied for E-plane and H-plane separately usually, if the antenna is linearly polarized. In Figure 2.3, the field components of the ideal dipole are demonstrated on a sphere and its radiation patterns are presented for E and H planes and in 3D.

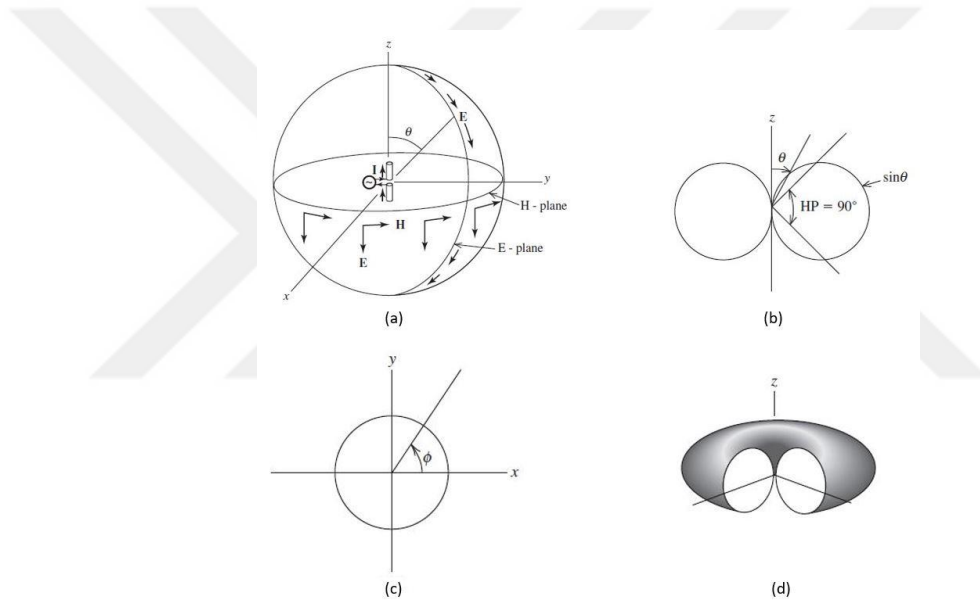


Figure 2.3: Radiation Representation for Ideal Dipole a) E and H Fields Vectors b) E-plane Radiation Pattern Polar Plot c) H-plane Radiation Pattern Polar Plot c) Radiation Pattern in 3D [24].

2.2.1 Radiated fields of an antenna

The fields are describes the surrounding area of the antenna and its definition depends on the r which indicates the position of observation point and the antenna position.

The radiated fields of an antenna defined as three regions; reactive near-field, radiating near-field (Fresnel) and far-field (Fraunhofer) regions. In Figure 2.4, the presentation of the fields is illustrated.

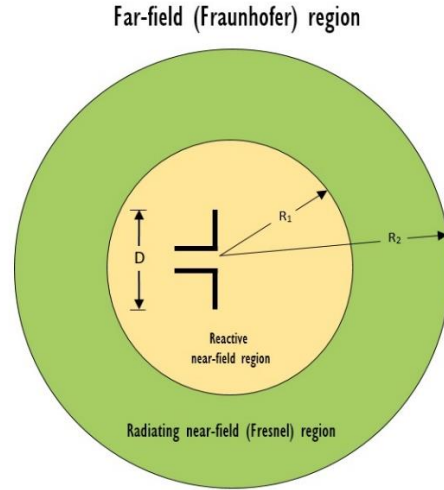


Figure 2.4: Field Regions.

The λ is the wavelength, D is the largest dimension of the antenna, also D value must be large with respect to the wavelength, and for reactive near field the distance is defined with Equation 2.28.

$$R_1 < 0.62\sqrt{D^3/\lambda} \tag{2.28}$$

The radiating near field (Fresnel) region locates between the near field and the farfield zone. The distribution of the field pattern has dependency on the radial component of r which is shown in Equation 2.29.

$$2D^2/\lambda > R_2 \geq 0.62\sqrt{D^3/\lambda} \tag{2.29}$$

The third region is the far-field region and the angular field distribution does not depend on the distance from the antenna. At the Figure 2.5, radiation amplitude behavior is demonstrated as a function of distance at the corresponding regions. As seen in Figure 2.5, the radiation main lobes occur more accurately as the distance goes for the far-field region.

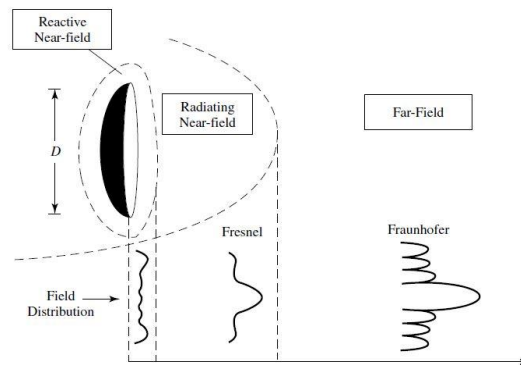


Figure 2.5: Radiation Characteristic with Respect to the Distance [24]

The antenna size is smaller than the wavelength means that the antenna is electrically small antenna. Otherwise, if the size of the antenna “D” is larger than the 2.5 times of the wavelength which means that the antenna is in the large antenna category. In this thesis, the studied antennas are small antennas and their far-field regions specified by considering under this conditions.

2.3 Basic Antenna Parameters

To describe the antenna implementation, in the sense of efficiency, capacity and performance, there are basic parameters must be used. The radiation pattern analyze is the first step to categorize the antenna. The radiation pattern is determined with respect to the application that the antenna will be used. These parameters are going to be explained in this chapter. Beamwidth, directivity, gain, and polarization are the criterias to define radiation pattern more specifically.

2.3.1 Radiation pattern

The radiation pattern of an antenna is defined as the change of the radiated electric field. The changes are expressed by mathemtaical functions and represented by graphes by using the space coordinates. The radiated electric field is spherical and the center is where the antenna locates. The spherical coordinate system has been used which is shown in the Figure 2.6. The radius of the sphere r , covers the antenna, is constant. Thus, the electric field has the only dependency on θ and Φ . This result that when the source is z-directed, then the electric field has only θ component, the normalized field pattern can be expressed as in Equation 2.30, where the $E_{\theta}(max)$ is the peak value of the magnitude of E_{θ} ;

$$F(\theta, \Phi) = \frac{E_{\theta}}{E_{\theta}(max)} \quad (2.30)$$

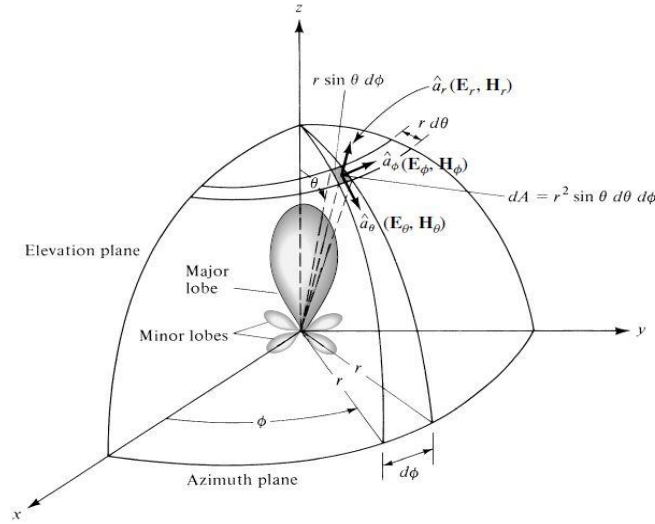


Figure 2.6: The Spherical Coordinate System Configuration for an Antenna [24].

The information means energy and the electromagnetic waves carry the information through a medium. That energy is explained by expressing the power which results from electric fields and named as an instantaneous Poytning vector that is shown in Equation 2.31.

$$\mathcal{W} = \mathbf{E} \times \mathbf{H} \quad (2.31)$$

where \mathcal{W} is instantaneous Poytning vector (W/m^2), \mathbf{E} is electric-field intensity (V/m), \mathbf{H} is instantaneous magnetic field.

To obtain the total power the \mathcal{W} should be integrated over the surface the energy flows. The expression of the time-varying power density and the avarage power density is represented in Equation 2.32.

$$\begin{aligned} \mathbf{P}_{rad} = \mathbf{P}_{av} &= \iint_S \mathbf{W}_{rad} \cdot d\mathbf{s} = \iint_S \mathbf{W}_{rad} \cdot \hat{\mathbf{n}} da \\ &= \frac{1}{2} \iint_S \text{Re}(\mathbf{E} \times \mathbf{H}^*) \cdot d\mathbf{s} \end{aligned} \quad (2.32)$$

If the radiated power is formulated over the solid angle which is shown the Figure 2.8, results the definition is named as ‘‘Radiation Intensity’’. In Equation 2.33 and 2.34, the solid angle expression is derived from surface area of a sphere. The expression of the radiation intesity is shown in Equation 2.33-3.25.

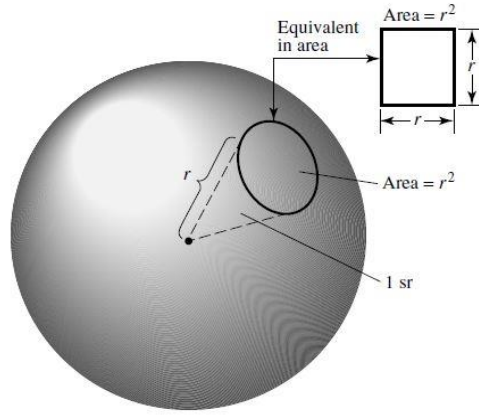


Figure 2.7: Solid Angle Definiton [24].

$$dA = r^2 \sin\theta d\theta d\Phi \text{ (m}^2\text{)} \quad (2.33)$$

$$d\Omega = \frac{dA}{r^2} = \sin\theta d\theta d\Phi \text{ (sr)} \quad (2.34)$$

$$U = r^2 W_{rad} \quad (2.35)$$

where the U is the radiation intensity with the unit $W/\text{unit solid angle}$, W_{rad} is radiation density with the unit W/m^2 . The antenna in far-field zone, the radial component may be neglected because of the small value compare to the angular components. As a result of this feature, the radiation intensity is defined with the power pattern that is presented in Equation 2.36.

$$P_{rad} = \iint_{\Omega} U d\Omega = \int_0^{2\pi} \int_0^{\pi} U \sin\theta d\theta d\Phi \quad (2.36)$$

where $d\Phi$ is the element of solid angle which equals to “ $\sin\theta d\theta d\Phi$ ” term. If an isotropic source is involved to equation, the radiation intensity will not depend on the angular components θ and Φ which indicated in Equation 2.37, as follows;

$$U_0 = \frac{P_{rad}}{4\pi} \quad (2.37)$$

2.3.2 Beamwidth

The antenna design is based on the analyze the beamwidth of the antenna. There is an opposite relation between the beamwidth and the sidelobe levels. The Half-Power Beamwidth (HPBW) is generally taken into account for analyzing the antenna radiation characteristics. The desired case for antenna radiation pattern is the

accumulate the power in the main lobe. The mathematical expression to define that case, the maximum side lobe level is compared to the maximum main lobe value. In Equation 2.38, the SLL means that side lobe level is defined as;

$$SLL_{dB} = 20 \log \frac{|F(SLL)|}{|F(max)|} \quad (2.38)$$

The half power beamwidth can be calculated by using Equation 2.39 where the $\theta_{HP \text{ left}}$ and $\theta_{HP \text{ right}}$ are points where the normalized power pattern has half of its value and the points are located on left and right of this value which is indicated in Figure 2.8.

$$HP = |\theta_{HP \text{ left}} - \theta_{HP \text{ right}}| \quad (2.39)$$

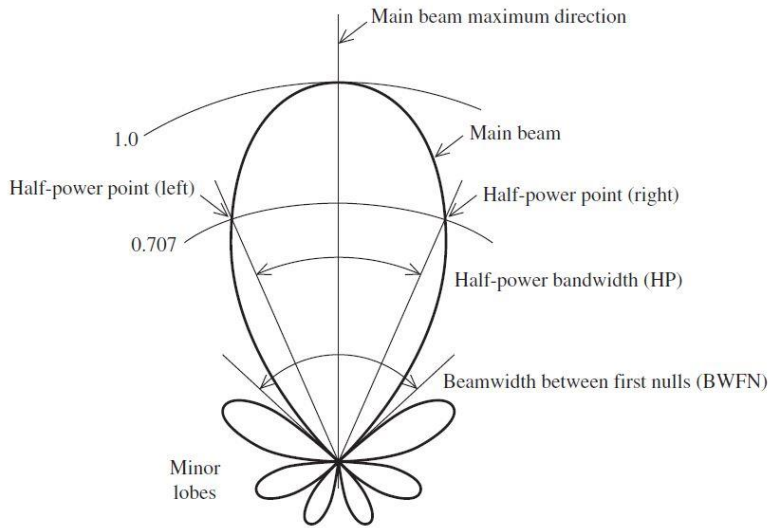


Figure 2.8: The Beam Classification Graph for Radiation Pattern of an Antenna [23].

2.3.3 Directivity

The directivity is defined by obtaining the ratio of the radiation intensity, which is in one direction, over the averaged radiation intensity over the overall area. When the direction is not specified is the case, then the maximum level of radiation direction is valid for the definition. The directivity is represented by using equation 2.40-41.

$$D = \frac{U}{U_0} = \frac{4\pi}{P_{rad}} \quad (2.40)$$

$$D_{max} = D_0 = \frac{U|_{max}}{U_0} = \frac{4\pi U_{max}}{P_{rad}} \quad (2.41)$$

where D is the directivity which has no dimension, D_0 is the maximum directivity.

The radiation patterns of an antenna mainly described by three different types; isotropic, directional, omnidirectional patterns. An isotropic radiation means that the power is equal in all directions. An omnidirectional pattern indicates that the power has equal value in a one of the E-plane or H-plane. The directional pattern of an antenna is expressed the amount of the power the radiation pattern has which is higher when it compares to the other directions of the radiation pattern.

The radiation patterns defined by using the principal patterns, which are the E- and H-plane patterns. The names indicates the Electric field and Magnetic field, the E-field where the electric field vector locates and the maximum level of radition is directed. The H-plane is similarly, where magnetic field vector locates and the maximum level of radiation is directed. In Figure 2.9, an omnidirectional radiation pattern is illustrated.

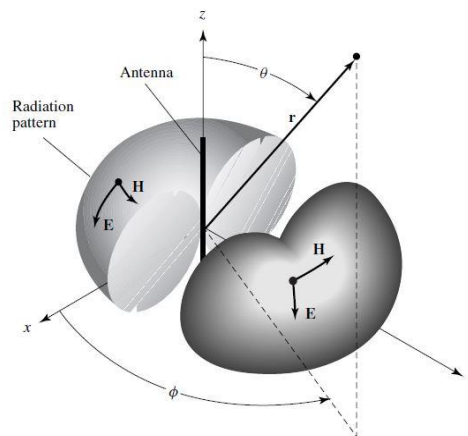


Figure 2.9: Omnidirectional Pattern [24].

2.3.4 Gain

Gain is important parameter to analyze the performance of an antenna. Because of the radiation incur losses during the transmission in a medium which is not the empty space, the gain define the how much power will be transmitted or received by the antenna itself. The mathematical definition is indicated as below in equation 2.42;

$$G = \frac{4\pi U_m}{P_m} \quad (2.42)$$

There some loses that are occurred due to effects of mismatches of impedance or polarization are not included in Equation 2.42. However, there is not only outside

effects, but also radiation power has losses because of the antenna design itself. This feature results a new definition which is the radiation efficiency. The radiation efficiency is defined as in equation 2.43-45.

$$e_r = \frac{P}{P_{in}} \tag{2.43}$$

where, $0 \leq e_r \leq 1$

$$G = e_r D \tag{2.45}$$

2.3.5 Input impedance, scattering parameters and bandwidth

The input impedance function has frequency dependency. The impedance can be defined between some specific frequency range. Besides that, the impedance is affected by antenna geometry, the feeding method of the antenna and the objects around the antenna. Because of the complexity of the antenna structure, the analytical solution of input impedance is not applicable for many kind of design. However, experimentally it can be solved and analyzed for the system compatibility.

The input impedance is also very important characteristic for the system the antenna is integrated. The antenna feeding mechanism is analyzed and matched according to the input impedance of the antenna. The scattering parameters define how the antenna input and output match well. Here, the input meets the input impedance and the output indicates the system the antenna is connected with. Thus, the input impedance is named as port in a network system, the voltage and current can be transferred between those ports. 50 Ω matches is desirable for general cases, for the experiments to perform the antennas operating frequency ranges by using the Network Analyzer. In Figure 2.10, a network is shown for two port system. The S-parameter matrix is expressed in Equation 2.46;

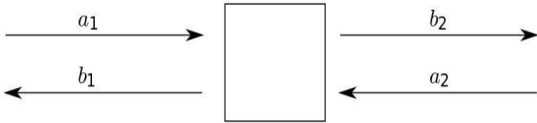


Figure 2.10: Two Port Network [25].

$$\begin{pmatrix} b_1 \\ b_2 \end{pmatrix} = \begin{pmatrix} S_{11} & S_{12} \\ S_{21} & S_{22} \end{pmatrix} \begin{pmatrix} a_1 \\ a_2 \end{pmatrix} \quad (2.46)$$

$$b_1 = S_{11}a_1 + S_{12}a_2$$

$$b_2 = S_{21}a_1 + S_{22}a_2$$

where the $a_1 = V_1^+$ and $a_2 = V_2^+$ which corresponds to the input voltage and $b_1 = V_1^-$ and $b_2 = V_2^-$ indicates the reflected voltage. From here, in equations 2.47-50, scattering parameters are derived.

$$S_{11} = \frac{b_1}{a_1} = \frac{V_1^-}{V_1^+} \quad (2.47)$$

$$S_{21} = \frac{b_2}{a_1} = \frac{V_2^-}{V_1^+}$$

$$S_{12} = \frac{b_1}{a_2} = \frac{V_1^-}{V_2^+}$$

$$S_{22} = \frac{b_2}{a_2} = \frac{V_2^-}{V_2^+} \quad (2.50)$$

Here, S_{11} and S_{22} correspond to the input power at the terminals where the antenna has feeding parts. The multiple input antennas have more than one scattering parameter. S_{12} and S_{21} define the correlation between the two input and the values are the same because of they are related to each other. In the antenna design steps, the S_{11} value has critical importance to understand the how much power transferred to the antenna structure. It is defined in dB scale mostly, and named also as reflected coefficient. The all power reflected means that no power transmitted which means S_{11} is equal to 0 dB. If the S_{11} equals to -10 dB, which is minimum desirable level for the antennas in mobile communication, when the accepted power 2 dB then the reflected power is -8 dB. In dB scale the calculation is done by equation 2.51 for the power and dB relation;

$$N_{dB} = 10 \log_{10} \frac{P_2}{P_1} \quad (2.51)$$

The S_{11} also defines the bandwidth which is the frequency interval where the antenna operates in. Under the -10 dB, all the frequency range included to operation bandwidth for the cases we interested. The width of the band where antenna works can be varied

with the purpose of the usage. Narrow band antennas can block the undesirable signals out of the frequency range as a result of that they have place such as GPS, security systems and RFID usages. Wideband and ultrawideband antennas operates at the widerange of the electromagnetic spectrum. Thus, it results high data transfer and wideband communication and mostly used in the radar applications. Bandwidth calculation can be done by using the upper and lower limits of the frequency range which is indicated in Equation 2.52 , where the F_H , F_L higher and lower frequency and F_C is the center frequency.

$$BW = 100 \times \frac{F_H - F_L}{F_C} \tag{2.52}$$



3. ANTENNAS

In the literature, there are many types of antennas categorized by the aim of the application, size, frequency range and the geometry. In this thesis, the main aim is to focus on mobile communication and 5G standards. For the reason of that, small antennas, directive and omnidirectional antennas, high gain antennas and array antennas are studied. Any kind of antenna type has own advantageous and disadvantageous. There is no only one type of antenna satisfy to all necessities. From to that point, 3 basic unit cells have been designed and after that, the designs are modified with the reflectors to obtain high gain. Directivity of the antennas are enhanced by using the array theory.

3.1 Microstrip Antennas

Microstrip antennas are low profile and they are convenient to integrate circuit board and electronic systems. They can be fabricated on PCB (printed circuit board), moreover, the fabrication can be done easily by using the printed technologies we have. A microstrip antenna contains a microstrip feeding line, where the name comes from, a ground plane and a patch part which is the responsible part for the radiation. Generally, the patch antennas refer to microstrip antennas in the literature. Microstrip antennas can be analyzed analytically for rectangular and circular patch types. In Figure 3.1, the microstrip antenna basics are presented.

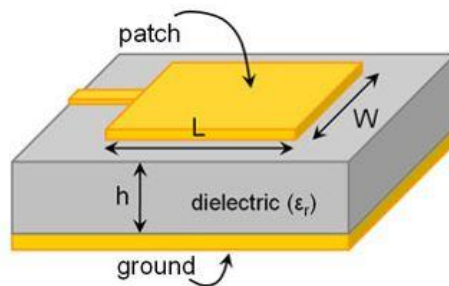


Figure 3.1: Microstrip Antenna Basics [26].

To obtain different radiation characteristics, the patch geometry can be adapted, modified and optimized for the desired frequency and size. Any shape has own radiation characteristics and should be determined for the purpose of the design. In Figure 3.2, a few patch shapes are presented.

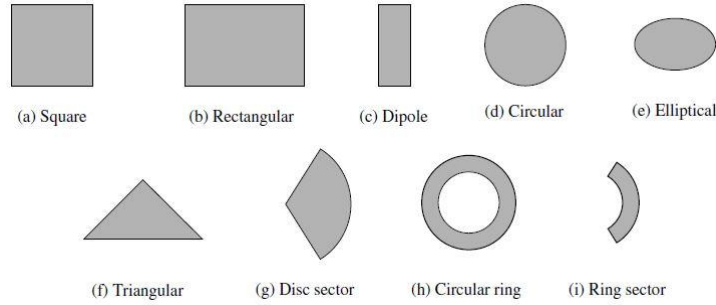


Figure 3.2: Different types of patch shapes [23].

The patch thickness and size, substrate thickness and dielectric constant and the feeding mechanism are parameters determine the radiation mechanism of the antenna. The equations 3.1- 3 show the critical points the microstrip antenna should be obeyed.

$$t \ll \lambda_0 \quad (3.1)$$

$$h \ll \lambda_0, \quad 0.003\lambda_0 \leq h \leq 0.05\lambda_0$$

$$\frac{\lambda_0}{3} < L < \frac{\lambda_0}{2} \quad (3.3)$$

The substrates that are used in the microstrip antenna design have dielectric constants between the range $2.2 \leq \epsilon_r \leq 12$. The dielectric materials that are used in this thesis study are given at the Table 3.1.

Table 3.1: Dielectric Substrates Properties.

Features	Name of Substrate	
	Fr-4 Epoxy	RT/duroid 6035HTC
Dielectric ϵ_r	4.4	3.5
Loss tangent δ	0.02	0.0013
Operation Frequency Range	Up to 6 GHz	8 GHz- 40 GHz

3.1.1 Rectangular patch antennas

The microstrip antennas have patch parts with different kind of geometries. The rectangular shape ease to analyze the analytical solution and fabrication of the antenna geometry. In Figure 3.3, the radiation principles are demonstrated and the coordinate system where the configuration located is presented.

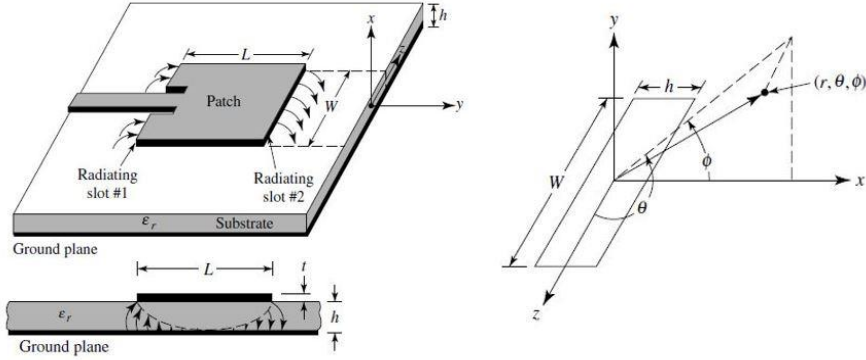


Figure 3.3: Rectangular Patch Antenna Configuration [24].

The rectangular patch antenna can be fed by microstrip line, probe feeding, proximity feeding and aperture coupling feeding. Feeding mechanisms will be explained in following chapter. However, the rectangular patch antenna with microstrip feeding is analyzed and the design parameter constraints can be obtained. Before presenting the equations, the fringing effect of the patch antenna should be explained due to understand effective dielectric constant. The electromagnetic waves which travel through slots located side of the patch create the fringing effect which is represented in Figure 3.3. As the $L/h \gg 1$ gets bigger the fringing effect is decreased. As the ratio between $W/h \gg 1$ gets bigger and $\epsilon_r \gg 1$, not the physical size but the electrical size of the patch gets larger. Because of that phenomena, ϵ_{reff} , effective dielectric constant, is introduced in the equations and it can be calculated by using equation 3.4 where $W/h > 1$. From here, the effective length L_{eff} can be represented as in equation 3.5.

$$\epsilon_{reff} = \frac{\epsilon_r + 1}{2} + \frac{\epsilon_r - 1}{2} \left[1 + 12 \frac{h}{W} \right]^{-1/2} \quad (3.4)$$

$$L_{eff} = L + 2\Delta L \quad (3.5)$$

In the design procedure, W and L , the actual lengths, should be determined by using the information of substrate dielectric, frequency in Hertz, and the height of the substrate h . In equations 3.6-7, the W and L calculations are shown.

$$W = \frac{1}{2f_r \sqrt{\mu_0 \epsilon_0}} \sqrt{\frac{2}{\epsilon_r + 1}} \quad (3.6)$$

$$L = \frac{1}{2f_r \sqrt{\epsilon_{reff}} \sqrt{\mu_0 \epsilon_0}} - 2\Delta L \quad (3.7)$$

3.1.2 Circular patch antennas

Unlike the rectangular patch antennas, the circular patch antennas can be optimized by changing only one variable, the r , the radius of the circle, so the frequency can be adjusted. The configuration of the circular patch antenna is represented in Figure 3.4. Similarly rectangular patch antenna, circular patch antennas have effective radius a_e which can be derived by using Equation 3.10. The dominant mode for the circular patch antenna is TM_{110}^z and its resonant frequency, f_r , can be calculated by using Equations 3.8-12.

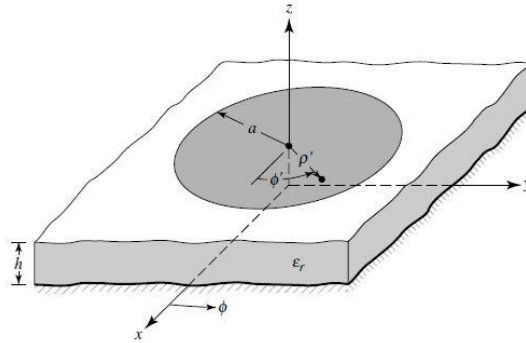


Figure 3.4: Circular Patch Antenna [24].

$$(f_r)_{mn0} = \frac{1}{2\pi\sqrt{\mu\epsilon}} \left(\frac{\chi'_{mn}}{a} \right) \quad (3.8)$$

$$(f_r)_{110} = \frac{1.8412}{2\pi a \sqrt{\mu\epsilon}}$$

$$a_e = a \left\{ 1 + \frac{2h}{\pi a \epsilon_r} \left[\ln \left(\frac{\pi a}{2h} \right) + 1.7726 \right] \right\}^{1/2} \quad (3.10)$$

$$a = \frac{F}{\left\{ 1 + \frac{2h}{\pi \epsilon_r F} \left[\ln \left(\frac{\pi F}{2h} \right) + 1.7726 \right] \right\}^{1/2}}$$

$$F = \frac{8.791 \times 10^9}{f_r \sqrt{\epsilon_r}} \quad (3.12)$$

3.1.3 Dipole and loop antennas

The dipole antenna is the basic geometry among the antenna designs and its analytical solution helps to construct the other designs. For that reason, electrically small dipoles have very common usage and also half wave dipoles are preferred more often than the other type of antenna geometries. A dipole antenna has an omnidirectional pattern which makes the dipole antenna convenient choice for mobile communication applications. The expressions which give the E and H components of the radiated fields are given between equations 3.13-17 and the configuration of the radiated fields and components are representation in Figure 3.5.

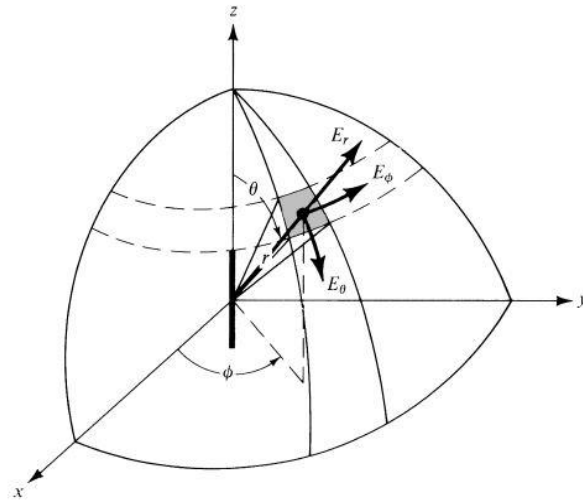


Figure 3.5: Electric Field Orientation of an Infinitesimal Dipole [24].

$$H_\phi = j \frac{I_0 k l \sin\theta}{4\pi r} \left[1 + \frac{1}{jkr} \right] e^{-jkr} \quad (3.13)$$

$$H_r = H_\theta = 0$$

$$\begin{aligned}
E_r &= \eta \frac{I_0 l \cos \theta}{2\pi r^2} \left[1 + \frac{1}{jkr} \right] e^{-jkr} \\
E_\theta &= j\eta \frac{kI_0 l \sin \theta}{4\pi r} \left[1 + \frac{1}{jkr} - \frac{1}{(kr)^2} \right] e^{-jkr} \\
E_\phi &= 0
\end{aligned} \tag{3.17}$$

Due to their feasible, cheap and practical adoption capabilities, loop antennas have many usages for different requirements. Loop antennas not only have electrically bigger size configuration, also electrically small sizes are preferable choices for different application needs. Loop antennas are used mostly in circular shape or rectangular shape because of the ease of analyzing and modeling. The analytical analyze for the loop antennas can be illustrated by assuming a linear dipole located at the center of the loop and acts as the reason for the radiation the loop creates. In Figure 3.6, loop configuration is shown, where a dipole is presented at the center of the loop.

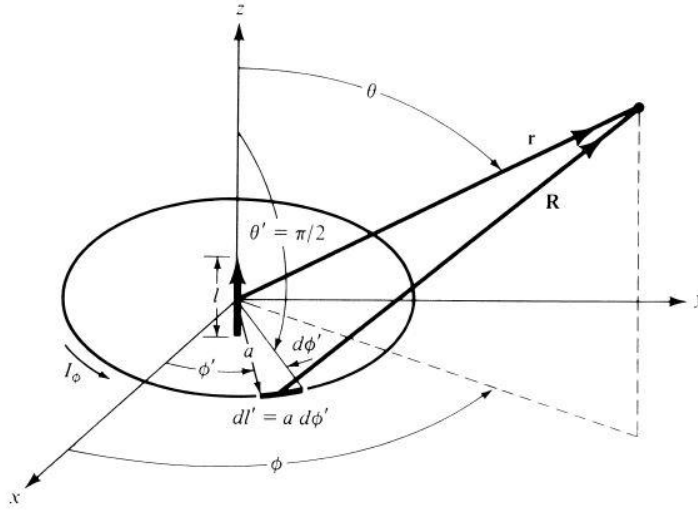


Figure 3.6: Loop Antenna [24].

For a small circular loop, because the size of the loop is too small, which means that the circumference C is less than 10λ , the radiation pattern is the same with a short dipole at far-field. However, its E and H -fields rely on the magnetic current which is assumed to flow on the dipole center at the loop. The equations are given as below;

$$E_\phi = \frac{\eta k^2 a^2 I_0 e^{-jkr} \sin \theta}{4r} \tag{3.18}$$

$$H_{\theta} = \frac{-E_{\theta}}{\eta} \quad (3.19)$$

3.2 Reflector Antennas

Reflector antennas have variety of geometrical shapes like curved or planar whis is indicated in Figure 3.7. In this thesis, the planar reflector plate is used to enhance the gain and directivity. Planar reflected antennas are explained by assuming the structure is designed by using two cell array antenna in a vertical arrangement. The theory behind this is the image theory which is shown in Figure 3.7 and formulated as seen in equation 3.19 and 3.20.

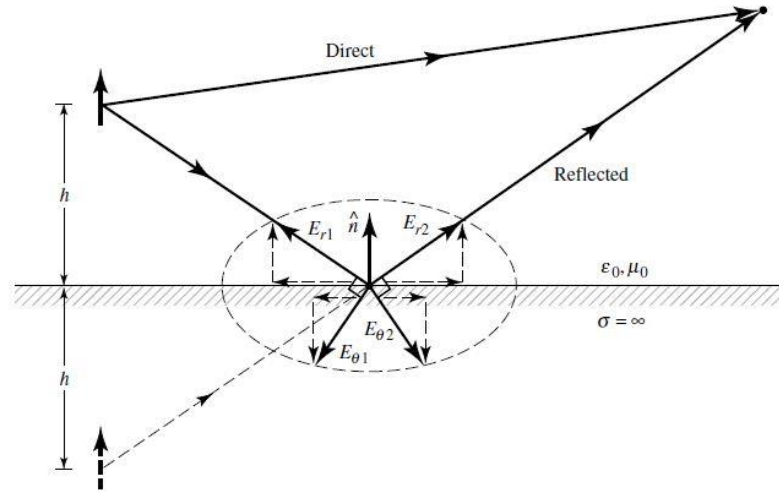


Figure 3.7: Image Theory Representation for E-Fields [24].

$$E_{\theta}^d = j\eta \frac{kI_0 l e^{-jkr_1}}{4\pi r_1} \sin\theta_1 \quad (3.19)$$

$$E_{\theta}^r = j\eta R_v \frac{kI_0 l e^{-jkr_2}}{4\pi r_2} \sin\theta_2 \quad (3.20)$$

The image sources are located below the PEC (Perfectly Electrical Conductor), but for real there is no field in this region. In the equations above, E_{θ}^d refers to direct electrical field and E_{θ}^r refers to reflected electrical field with the term R_v is the reflection coefficient.

3.3 Array Antennas

By increased demand for the long-distance wireless communications systems, the array antennas become very popular due to their high gain feature. Array antennas are mostly used to transform the beam to obtain more directed radiation pattern. Especially, with the 5G, millimeter-wave antennas should be designed with very high gain because of their high loss characteristics when they travel in a medium. Array antennas provide more directed and increased gain radiation beams by accumulating the radiation in one direction. There are different ways to design array antennas which can be linear, circular, rectangular etc. Moreover, by setting the distance between elements, the radiation pattern and side lobes can be adjusted. Besides that, applying phase difference to each element, the radiation pattern can be also redesigned in some sense. For two infinitesimal dipole, which is presented in Figure 3.8, the total field can be written which is indicated in Equations 3.21-22 where the β is the phase difference between elements.

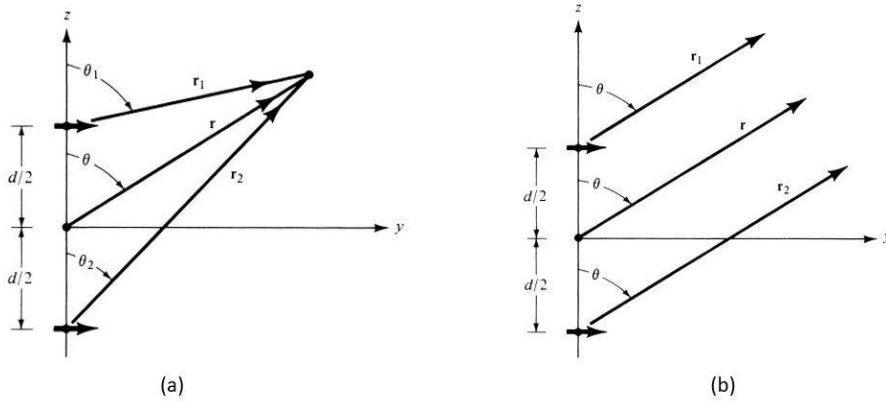


Figure 3.8: Array Configuration a) Two Dipole b) at Far-Field [23].

$$E_t = E_1 + E_2 = \hat{a}_\theta j\eta \frac{kI_0 l}{4\pi} \left\{ \frac{e^{-j[kr_1 - (\frac{\beta}{2})]}}{r_1} \cos\theta_1 + \frac{e^{-j[kr_2 - (\frac{\beta}{2})]}}{r_2} \cos\theta_2 \right\} \quad (3.21)$$

For far-field observation equation becomes;

$$E_t = \hat{a}_\theta j\eta \frac{kI_0 l e^{-jkr}}{4\pi} \cos\theta \left\{ 2 \cos \left[\frac{1}{2} (kdcos\theta + \beta) \right] \right\} \quad (3.22)$$

The term $\left\{ 2 \cos \left[\frac{1}{2} (kdcos\theta + \beta) \right] \right\}$ is called the array factor for two element have same amplitude. It can be seen from the equation above that the total field is the

multiple of the array factor with the E-field for the one element. The array factor is shown in normalized form in Equation 3.23.

$$(AF)_n = \cos \left[\frac{1}{2} (kdcos\theta + \beta) \right] \quad (3.23)$$





4. ANTENNA DESIGN

From theory to fabrication, an antenna design have complex steps to study on. The geometry of the antenna can be specified by taking into account expected radiation pattern properties. One of the very important parameter for an antenna design is the feeding method. Feeding mechanism should be coherently with the overall design. After composing the geometry and the feeding method, the antenna should be simulated by using one of the numerical methods or hybrid methods. There are different commercial programs that run the electromagnetic simulations. However, in this thesis, the simulations are realized by using the HFSS (high frequency simulation software) and CST (Computational Simulation Tool).

4.1 Feeding Mechanism

By considering the most effective feeding method for a patch antenna should be combined with a feeding part. In most cases, the feeding point is matched to 50Ω . There are four main feeding techniques which are microstrip feeding, probe feeding, proximity feeding, and aperture coupling method. However the most common method is the microstrip feeding, all methods have distinct properties.

4.1.1 Microstrip feeding

The microstrip feeding method is easy to apply to patch antennas and it is practical for fabrication procedure. The microstrip feed line can be extended from the point where the antenna can be fed from which is shown in Figure 4.1. The matching quality can be adjusted by changing the position and length of the inset location. In the designs that studied in this thesis, the microstrip feeding method is applied for different antenna designs. All the feed lines are matched to 50Ω .

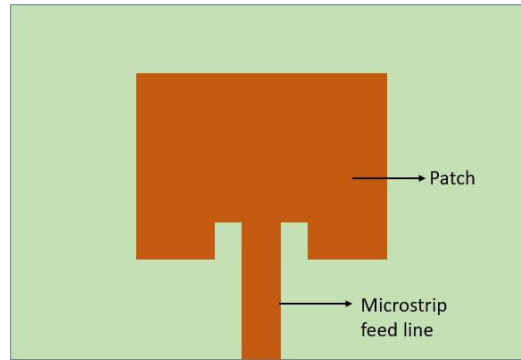


Figure 4.1: Microstrip Feeding Line.

4.1.2 Probe feeding

The probe feeding is also an intersect feeding like microstrip line feeding method. The probe feeding is also named coaxial feeding which the outer conductor of the probe is attached to ground plane and the origin of the probe reach to the radiating patch. In Figure 4.2, probe feeding scheme is introduced. For the substrates with the high thickness value, modeling and fabricating the antenna is more difficult than the microstrip feeding method.

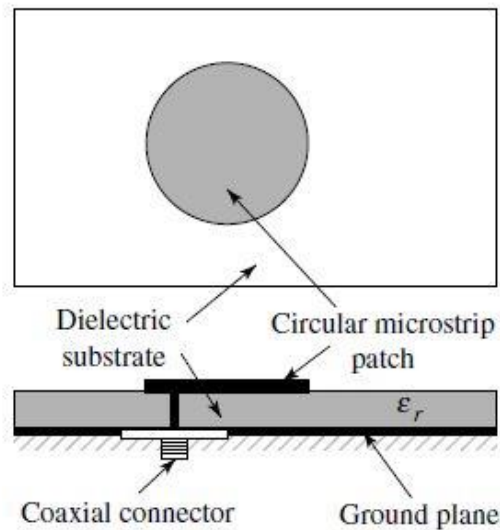


Figure 4.2: Probe Feeding [24].

4.1.3 Proximity feeding

Other than the intersect feeding methods, the proximity feeding is a method that radiating element and input line does not touch each other. In Figure 4.3, proximity

feeding presentation is indicated. The feed line is located between the dielectric substrate and it excites the patch without touching.

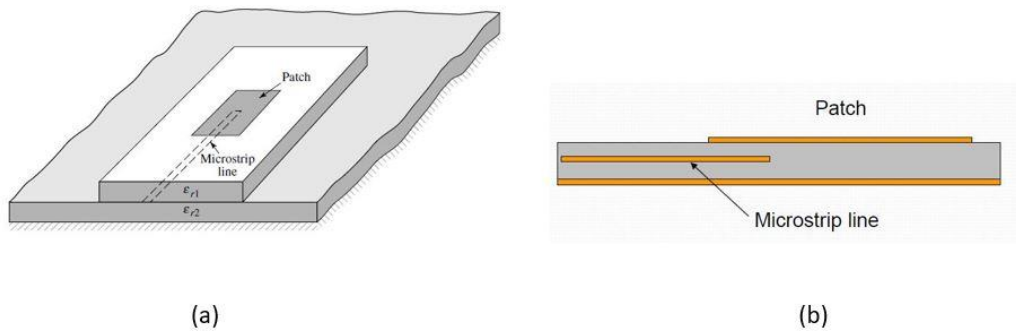


Figure 4.3: Proximity Feeding a) from Top, b) from Side View [24].

4.1.4 Aperture coupling feeding

The aperture coupling feeding method consists of two different dielectric substrates that are apart from each other with a ground plane. A slot located on the patch provides the excitation reaching the patch via the ground plane. Using the aperture coupling, feeding mechanism, slot position, and the radiating patch can be optimized independently. For combining two different characteristics dielectric material, generally, the higher dielectric substrate is located at the bottom and the lower one is located at the top. In Figure 4.4, an aperture coupling feeding mechanism is illustrated.

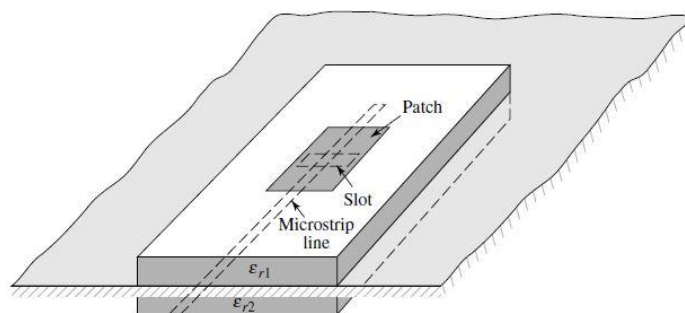


Figure 4.4: Aperture Coupling Method [24].

4.2 Simulation Techniques and Tools

The reasons behind the need for designing a new antenna can be listed as enhancing or optimizing the system capability, efficiency or size, etc. Since the theory and the real-life does not match completely and also the complexity of the antenna does not let to analyze the antenna analytically, the designed antenna should be analyzed by using the numerical techniques. Finite element, finite difference time domain, method of moments are names some of the most common numerical techniques. However, some hybrid methods are also used for analyzing the antennas. Although it is possible to have these techniques by coding them and apply them to the desired geometry, there are some commercial software programs let us make electromagnetic simulations, user-friendly. HFSS (High Frequency Simulation Software) and CST Microwave Studio Program are widely used among the antenna designers. In this thesis, both software program is used to simulate the antennas.

4.2.1 HFSS (High Frequency Simulation Software)

Anslys HFSS is a commercial program allows us to design and realize electromagnetic simulations by using different solvers for different needs. By using the HFSS, high-frequency electronic products can be designed, for example; antennas, antenna arrays, filters or components, etc. 3D model can be created and then, it can be analyzed by using electromagnetic solvers, such as; finite element solver or integral equation solver which based on numerical techniques those are FEM (Finite Element Method), MoM (Method of Moment). In Figure 4.5, two of example which solved by applying different solvers is illustrated.

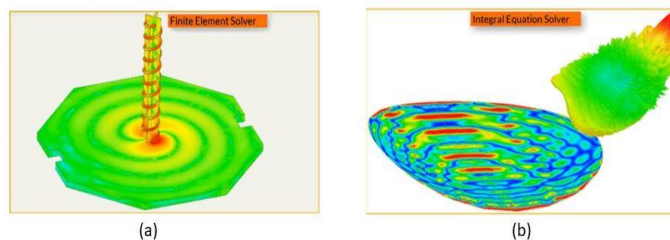


Figure 4.5: HFSS Radiation Simulations [28]

To simulate an antenna cell in HFSS, there are some steps that should be followed. The real scenarios require more complex antenna design, in most of the cases. Because of that reason, antenna parameters should be optimized for different boundary

conditions and different geometrical combinations despite the fact that the parameters had been calculated by using the theoretical equation. After the radiating element is combined with the convenient feeding mechanism, the excitation method should be specified. For the designs that the thesis includes, a lumped port is used for the excitation. To assign the radiation boundary is the second step before to start the simulation. For far-field calculations, boundary size should exceed at least quarter wavelength.

4.2.2 CST microwave studio program

Another high frequency electromagnetic simulation software program is the CST microwave design and analyze program. CST has very similar features compared to the HFSS. However, there are some advantages CST has. One of them is more than one mesh-type; hexahedral grids and tetrahedral grids. The second advantage of CST is that having diverse solvers for different types of problems, such as; transient solver, frequency-domain solver, integral equation solver [29]. In Figure 4.6, a simple geometry that is meshed with hexahedral grids is illustrated.

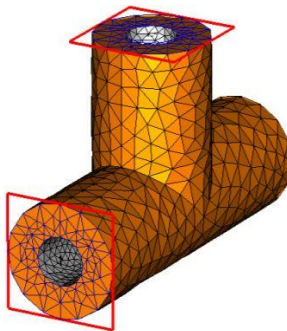


Figure 4.6: CST Mesh Configuration [29].

The design procedure in CST is very similar to all other 3D CAD programs. Unlike the HFSS uses FEM in its background, CST works with the FDTD. Both numerical techniques solve the maxwell's equations in differential or integral form. It is important that the specify the geometry requirements to determine which solver is convenient for the analyze. In the end, both simulation programs should give the converged answer for the same designs with the same boundary conditions.



5. DUAL BAND QUASI-YAGI ANTENNA

Increasing demand for mobile communication systems with 5G requires to solve new problems. For instance, high data transfer, compact and effective designs are the challenges that may be taken as a priority to being improved. A dual-band quasi-yagi antenna design provides two different applications by covering two different bands. One of them is 2.4 GHz Wi-Fi band and the other one is 3.5 GHz that is the upcoming 5G mobile communication band. The referenced design [12] has been simulated and fabricated to compare with the improved design solutions. The model has been advanced by designing two element array with two inputs. Then the unit cell has been evolved to four element array with two input by adding power divider path on the same design. At the final stage of the study, the reflector plate is added to structure to have a virtual array in a sense, by doing this procedure so the gain is enhanced for unit cell and two element design. By arraying the system, the directivity and the gain improvement has been aimed.

5.1 Single Element Design

The dual band antenna [12] has ben designed on FR-4 substrate that has the 4.4 dielectric constant. The FR-4 dielectric substrate features have been presented previously in table 3.1. The designed antenna is presented in Figure 5.1 and the parameters of the design geometry are given at Table 5.2 below. The operating bands of the dual band antenna have 2.3 GHz and 3.5 GHz center frequencies, respectively. As a result of having two different radiating geometry, two different radiation pattern is occured. In following equations 5.1 and 5.2, W_d defines the length of the dipole and W_{loop} defines the total size of the loop geometry. In Figure 5.2, the fabricated antenna can be seen.

$$W_d = \frac{0.35 \times c}{f_{dipole}} \quad (5.1)$$

$$W_{loop} = \frac{0.20 \times c}{f_{loop}} \quad (5.2)$$

The antenna has a compact size of $38 \times 19 \text{ mm}^2$ which corresponds to $0.045 \lambda_{loop}^2$. All of that, the loop geometry length corresponds to $0.208 \lambda_{loop}$, as total and the dipole has $0.353 \lambda_{dipole}$ length where λ_{loop} , λ_{dipole} are 125mm and 85 mm for center frequencies, respectively.

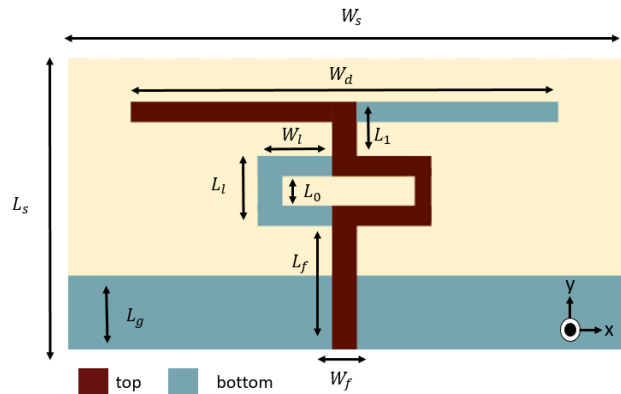


Figure 5.1: Unit Cell Quasi-Yagi Antenna.



Figure 5.2: Fabricated Unit Cell Antenna.

Table 5.1: Antenna Parameters.

Parameter Name	Length	Parameter Name	Length
L_g	5 mm	W_l	4 mm
L_0	0.5 mm	W_f	1.5 mm
W_s	38 mm	L_f	8.75 mm
L_s	19 mm	L_1	3.5 mm
L_l	3.5 mm	W_d	30 mm

The

length of the microstrip line is 8.75mm and the ground plane has height as 5mm. The antenna feed line has been designed to be matched to 50Ω .

To analyze the performance of designed antenna there are parameters should be determined. One of the most important parameter is the S_{11} , which is the scattering parameter that defines the quantity of the delivered and scattered power. 2D and 3D radiation patterns are simulated and performed experimentally for this reference design.

5.1.1 Simulation and experimental results

In Figure 5.3, 3D radiation patterns of unit cell antenna is presented. The gain for 2.3 GHz is 1.2 dB and 5.2 dB for 3.5 GHz. In Figure 5.4, scattering parameter graph is indicated. The peak values are shown in Table 5.2.

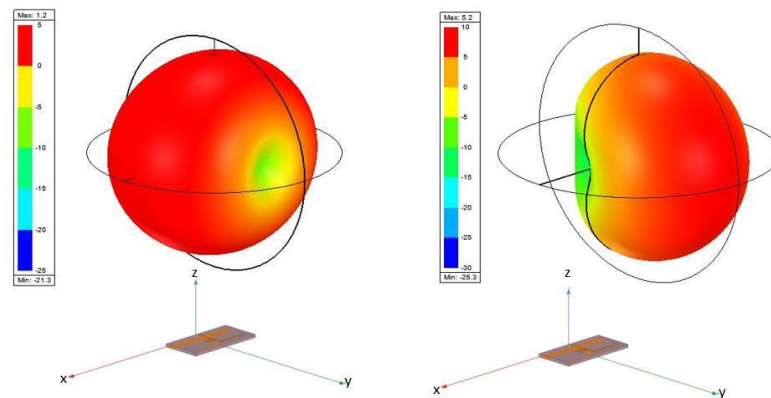


Figure 5.3: 2D and 3D Simulated Radiation Pattern for Unit Cell (a) and (b) for 2.3 GHz; (c) and (d) for 3.5 GHz

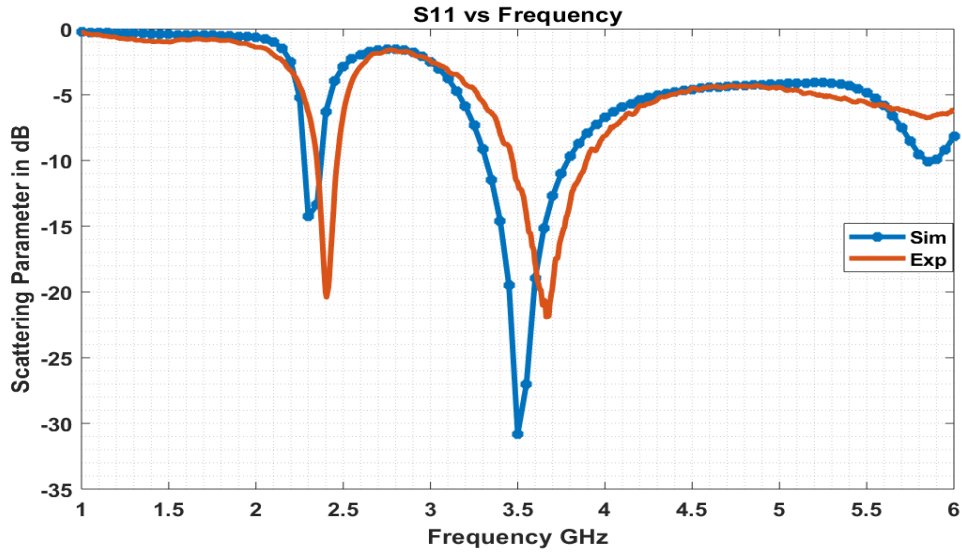


Figure 5.4: S_{11} vs Frequency Graph for Simulated and Experimental Data.

Table 5.2: Peak Values for S_{11} .

Geometry	Simulation Result		Measurement Data	
	Frequency (GHz)	S_{11} (dB)	Frequency (GHz)	S_{11} (dB)
	2.3	-17.65	2.44	-12.13
	3.5	-31.69	3.7	-35.36

5.2 Two Element Array Design

After the unit cell has been designed and fabricated, as a second stage, the design has been adopted to 1x2 array for the purpose of having more directive and increased gain features. Moreover, having multiple inputs on the structure gives the ability to control the phase and amplitude of the input signal for different individual antenna. However this part is not included in this thesis. The array is modelled with the same specifications with the unit cell. The distance between two cell is studied parametrically by taking the account the array factor effect. In Figure 5.5, the array structure is represented where “d” refers to distance between the ground planes and “ d_a ” refers to main distance between radiated structure.

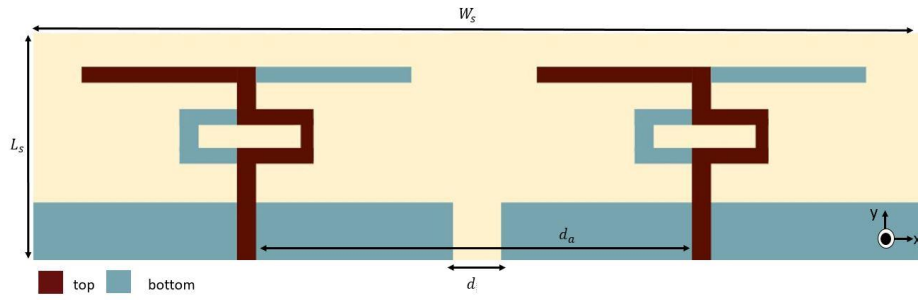


Figure 5.5: 1x2 Array Antenna Design.



Figure 5.6: Fabricated Antenna.

While performing the parametrical study of "d", the values calculated by considering the wavelength of lower frequency 2.3 GHz which is 130mm. Initial value of the d_a is equal to 36.5 mm when d equals to 0. Therefore, the sum of d and the initial distance between the antennas increase the d_a values.

For multiple input arrays, not only S_{11} but also S_{21} parameters have importance because of the correlation between two input may affect the total radiation pattern and antenna matching. In Table 5.3, the effects of distance on scattering parameter and maximum gain are listed.

Table 5.3: Parametric Results vs Distance.

Distance (mm)	$d = 0;$ $d_a = 0.28\lambda_{loop}$		$d = 19;$ $d_a = 0.4\lambda_{loop}$		$d = 28.5;$ $d_a = 0.5\lambda_{loop}$		$d = 35;$ $d_a = 0.55\lambda_{loop}$		$d = 61;$ $d_a = 3\lambda_{loop}/4$		$d = 93.5;$ $d_a = \lambda_{loop}$	
Frequency (GHz)	2.3 (GHz)	3.5 (GHz)	2.3 (GHz)	3.5 (GHz)	2.3 (GHz)	3.5 (GHz)	2.3 (GHz)	3.5 (GHz)	2.3 (GHz)	3.5 (GHz)	2.3 (GHz)	3.5 (GHz)
Gain (dB)	2.4 dB	5.5 dB	3.8 dB	7.6 dB	4.5 dB	7.9 dB	4.9 dB	8.0 dB	5.2 dB	7.8 dB	4.6 dB	7.8 dB
S_{11} (dB)	-6.28 dB	-30.44 dB	-12.69 dB	-32.68 dB	-16.17 dB	-35.39 dB	-14.26 dB	-31.02 dB	-15.5 dB	30.12 dB	-15.07 dB	-29.39 dB
S_{21} (dB)	-13.40 dB	-16.22 dB	-12.61 dB	-23.21 dB	-14 dB	-25.31 dB	-18.43 dB	-26.20 dB	-17.83 dB	-30.72 dB	-21.79 dB	-32.75 dB

In Figure 5.7, 3D radiation patterns are represented and the gain values are 4.9 dB and 8 dB for corresponding frequencies 2.4 and 3.5 GHz, respectively.

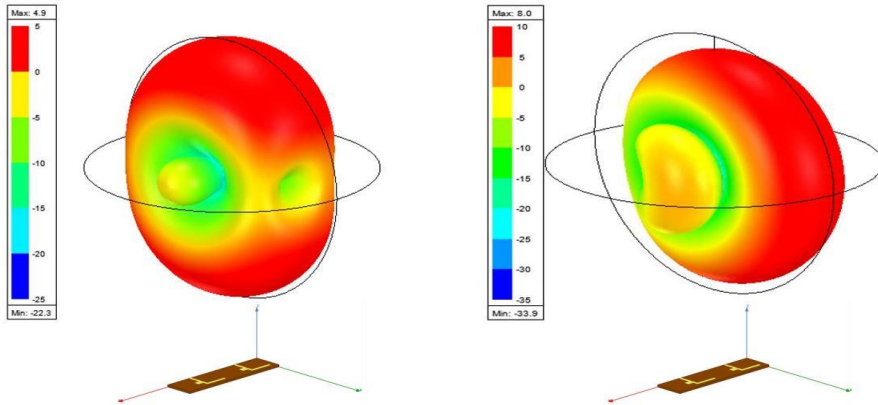


Figure 5.7: 3D Radiation Pattern of Two Element Array.

In Figure 5.8, the current distributions are demonstrated for lower and upper frequencies, respectively.

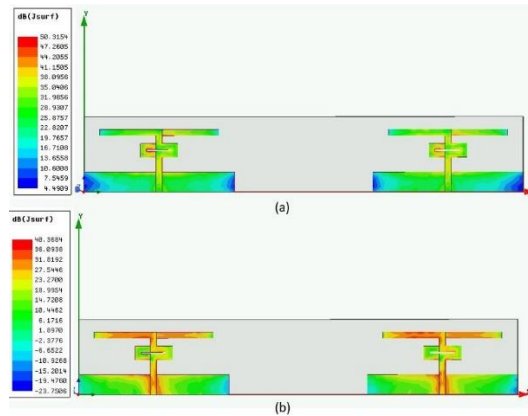


Figure 5.8: Current Density of Two Element Array (a)2.3 GHz and (b)3.5 GHz.

As seen in the Figure 5.9, the simulated scattering parameters S_{11} and S_{21} matches well with the experimental measurements. Both simulated and experimental data for S_{11} below the -15 dB which is good candidate for mobile communication systems. S_{21} values should be expected above the -20 dB which means no correlation to restrain antennas performance.

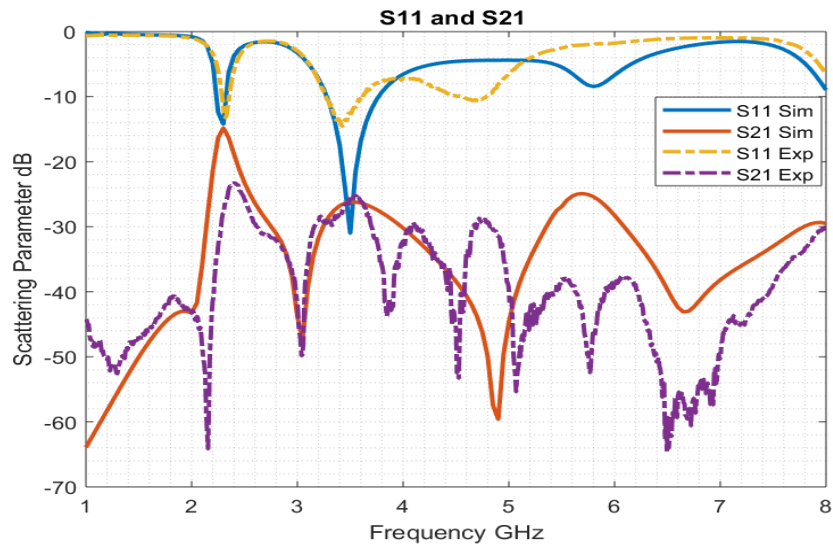


Figure 5.9: S_{11} and S_{21} Values.

5.3 Four Element Design

The purpose to design four element antenna is having more directive antenna to use in beamforming applications. In this design, despite the preserve radiation characteristics, the power divider that connect the two element only feasible for 3.5 GHz band. However, in experimental measurements, the antenna matches around -15 dB for 2.3 GHz. In Figure 5.10, the design parameters are illustrated. In Table 5.4, the values with corresponding parameters are written.

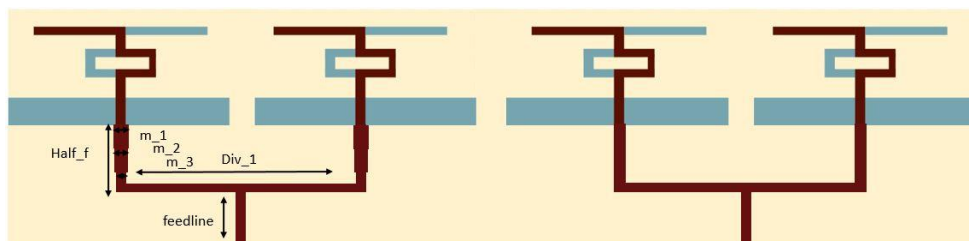


Figure 5.10: Four Element Antenna Design.

Table 5.4: Parameter Values.

Parameter Name	Length on X direction	Length on Y direction	Parameter Name	Length on X direction	Length on Y direction
Half_f	18 mm	-	M_1	1.75mm	10mm
Div_1	74 mm	1mm	M_2	1.5 mm	5 mm
Feedline	5mm	2.5 mm	M_3	1 mm	3mm

5.3.1 Simulation and experimental results

The fabricated antenna is pictured in Figure 5.11, and the scattering parameters S_{11} and S_{21} are shown in Figure 5.12. In the scattering parameter graph, the experimental and simulated data is presented, coherently. Besides that, S_{11} value is seem shifted compared to the simulated data. The reasons are that it could be the material quality and the fabrication and measurement imperfections.

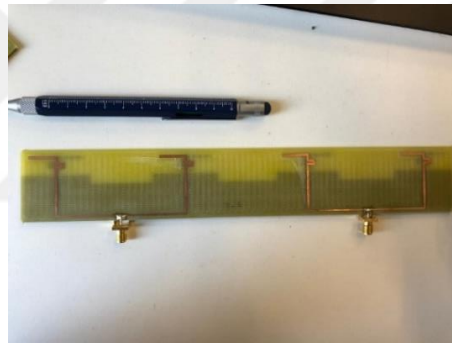


Figure 5.11: Fabricated Antenna.

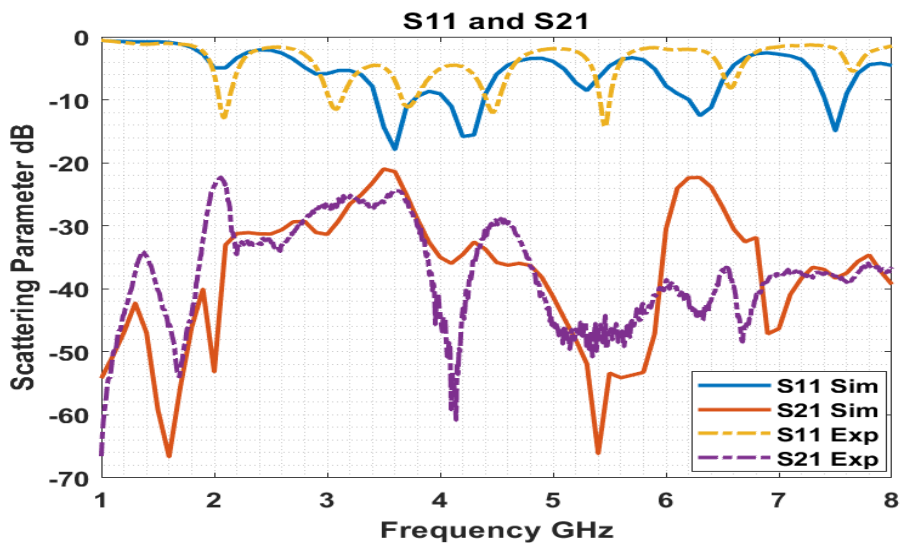


Figure 5.12: S_{11} and S_{21} Values.

In 3D radiation pattern, the maximum gain is 6.2 for 2.3 GHz and 8.3 dB for 3.5 GHz. As seen from the pattern, the directivity is very narrow compared to the two element array design. The gain is expected to be higher, but the mismatching of the power divider affects the gain.

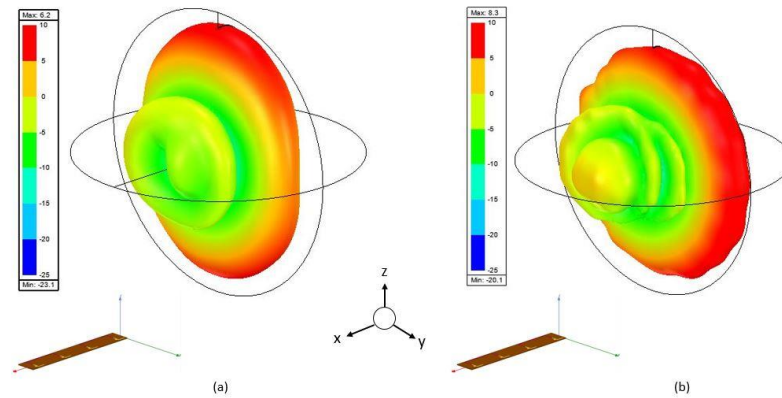


Figure 5.13: 3D Radiation Pattern (a) 2.3 GHz and (b) 3.5 GHz.

5.4 Virtual Array Design

By using the reflector plate, virtual array design can be obtained to enhance the gain with a basic application. For unit Quasi-Yagi antenna and two element Quasi-Yagi antenna, reflector plates are optimized to minimize the side lobes and the gain is increased for both antenna design.

5.4.1 Unit cell antenna

The fabricated antenna is configured with a reflector plate with optimized values for length and height. The radiation patterns are measured in anechoic chamber as shown in Figure 5.15, to obtain far-field radiation characteristics. The result of the measurements are presented in 2D in E and H-planes.



Figure 5.14: Fabricated Unit Cell Antenna.



Figure 5.15: Anechoic Chamber and Far-Field Measurement for Fabricated Antenna.

The gain is increased from 1.3 db to 6.52 dB for 2.3 GHz and from 5.8 db to 8.3 dB, in virtual array with compared to the unit cell. The 3D radiation patterns are indicated in Figure 5.16.

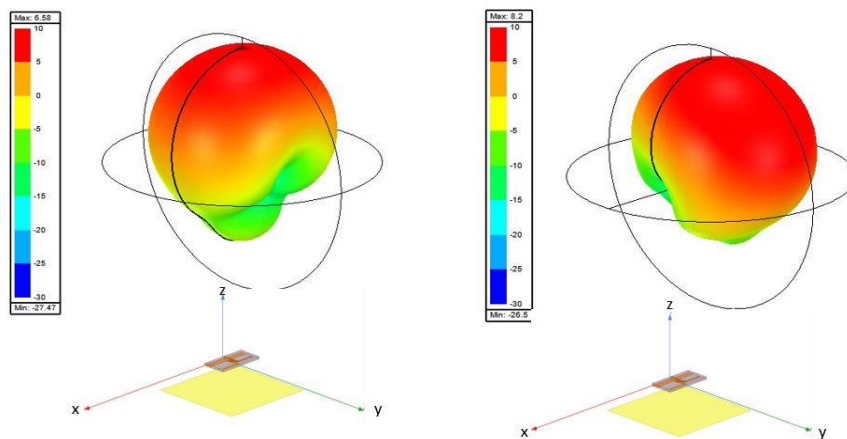


Figure 5.16: 3D Radiation Pattern (a)2.3 GHz and (b) 3.5 GHz.

Parametrical study is represented with 2D graphs because to see effects of different values for “L” length and “h” height on the radiation pattern on E and H-fields, respectively. In Figure 5.17 the L values are shown and in Figure 5.18 h values are demonstrated.

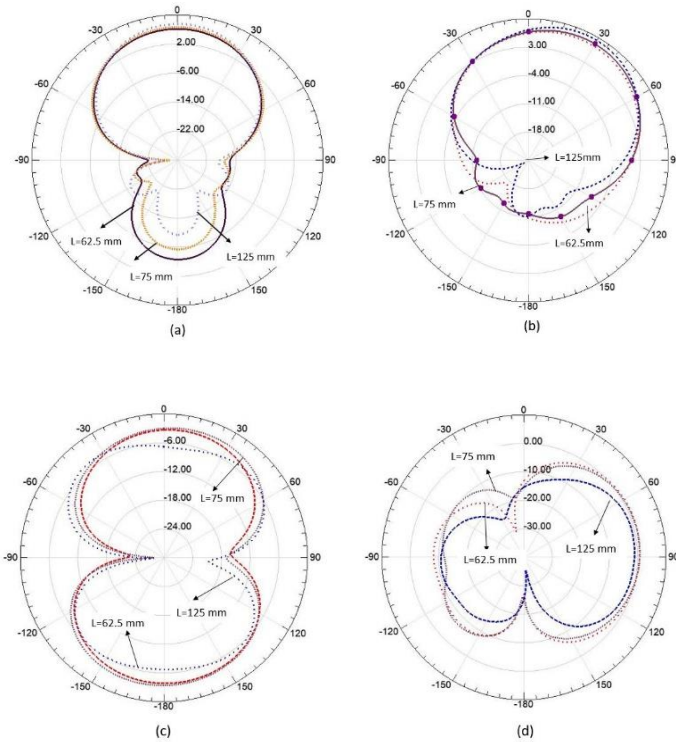


Figure 5.17: Simulated 2D Radiation Pattern for Different “L” Values (a),(b) 2.3 GHz and 3.5 GHz in E-plane; (c),(d) 2.3 GHz and 3.5 GHz in H-plane.

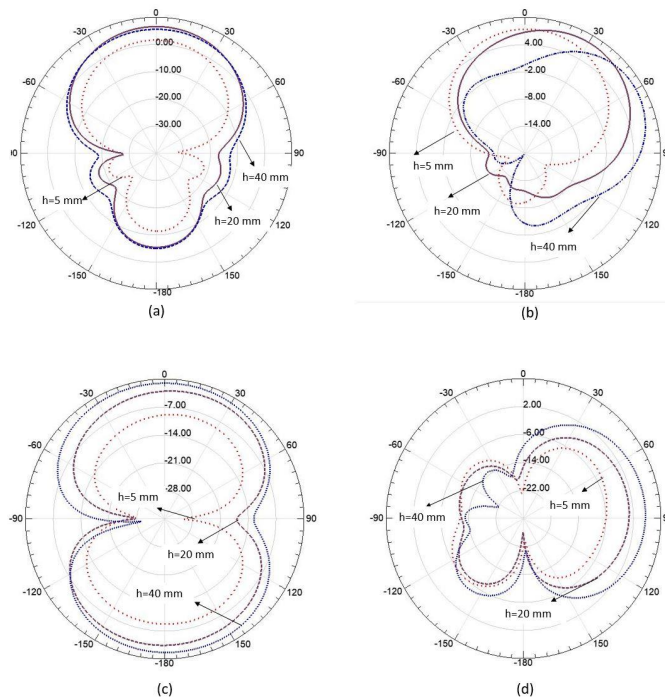


Figure 5.18: Simulated 2D Radiation Pattern for Different “h” Values (a),(b) 2.3 GHz and 3.5 GHz in E-plane; (c),(d) 2.3 GHz and 3.5 GHz in H-plane.

In the Figure 5.19, the experimental radiation pattern data and simulated data are sketched together. As seen in the Figure 5.19, the experimental and simulated radiation pattern have similar characteristics.

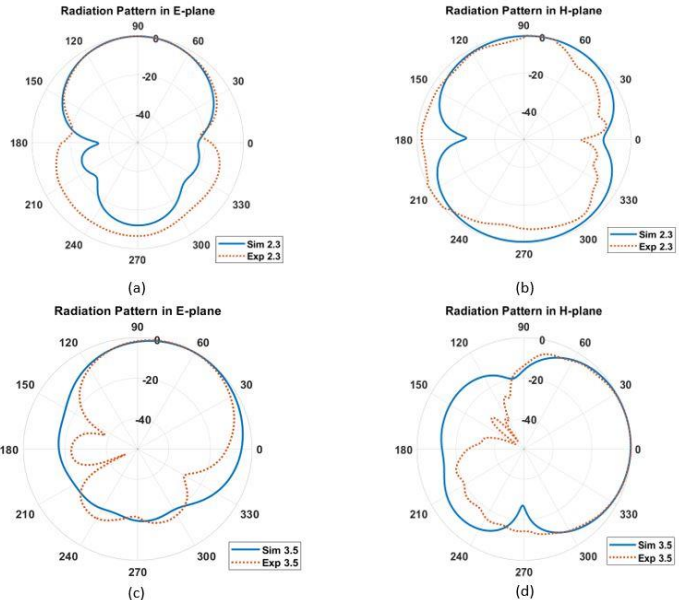


Figure 5.19: Experimental Results of the Radiation Pattern for a),b) E and H planes without Reflector c),d) E and H plane with Reflector.

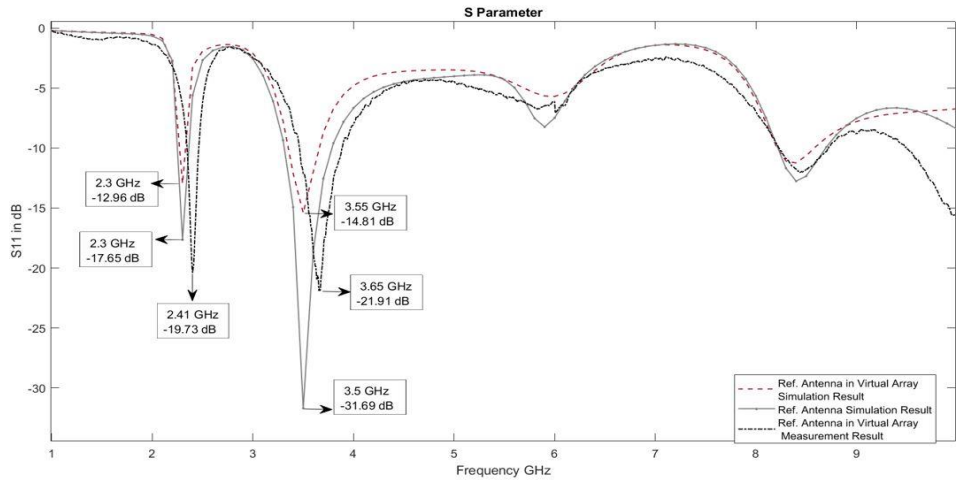


Figure 5.20: S_{11} Values.

5.4.2 Two element array antenna

By adding the reflector plate in the two element antenna design, the gain is enhanced successfully. The gain for 2.3 GHz is increased from 4.9 dB to 10.1 dB and from 8 dB to 13.2 dB for 3.5 GHz. In Figure 5.20, 3D radiation pattern are shown for corresponding frequencies.

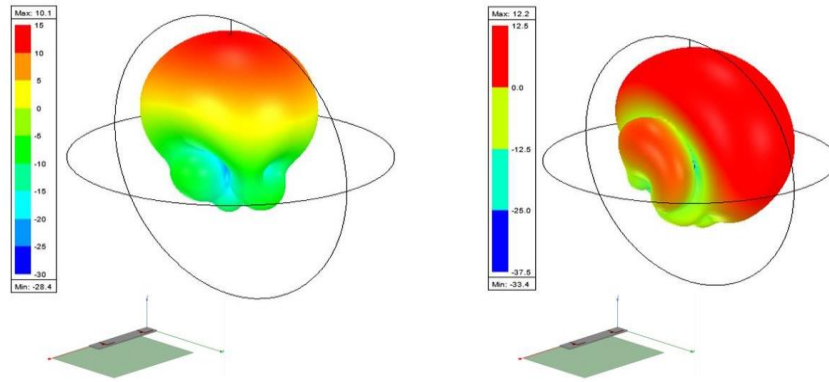


Figure 5.21: Simulated 3D Pattern and Antenna Configuration a) 2.3 GHz and b) 3.5 GHz.

By changing the length of the reflector plate, the side lobe reduction is realized. In Figure 5.21, 2D radiation pattern results are presented. Both E-plane and H-plane patterns are illustrated for 2.3 GHz and 3.5 GHz. In Figure 5.22, the effects of adjusted parameter “h” is pictured.

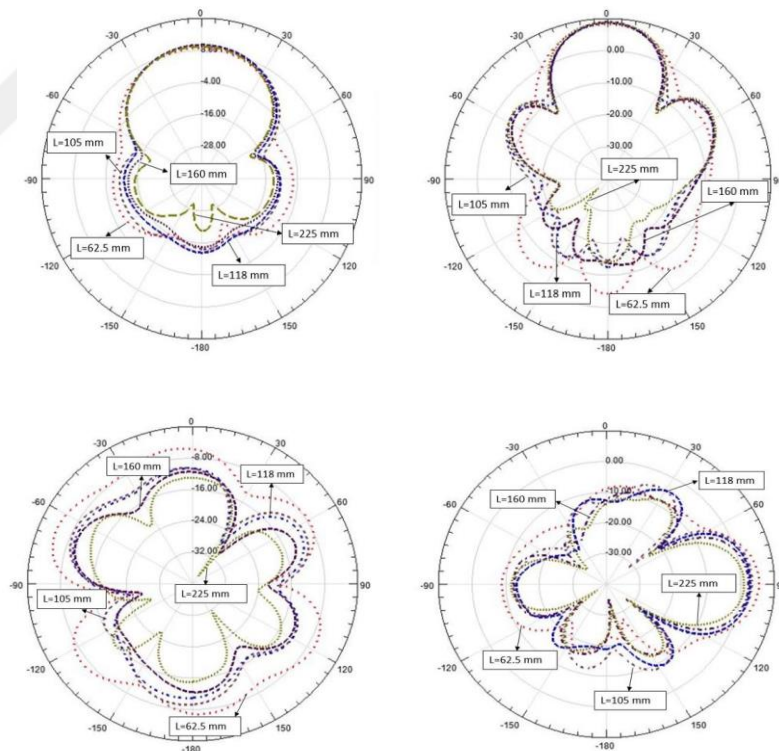


Figure 5.22: “L” Length Of The Copper Reflector Plate (a) 2.3 GHz (b) 3.5 GHz for E-plane ($\Phi=0^\circ$) ; (c) 2.3 GHz 5 GHz for H-plane ($\theta=90^\circ$).

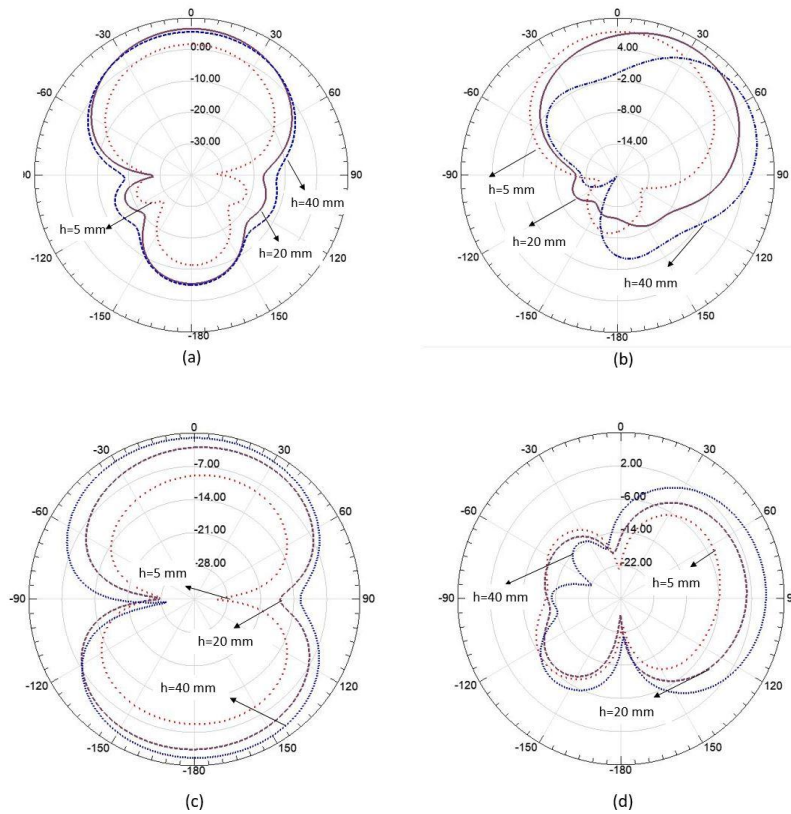


Figure 5.23: “h” Parametrical Result in 2D Radiation Pattern (a) 2.3 GHz and (b) 3.5 GHz at the E-plane ($\Phi = 90^\circ$) and (c) 2.3 GHz and (d) 3.5 GHz at the H-plane ($\theta = 0$) for $L = 75\text{mm}$; $h = 5\text{mm}$; 20mm ; 40mm .

The current distribution is shown in Figure 5.23 and the effect of the reflector plate is presented in the graphs for 2.3 GHz and 3.5 GHz.

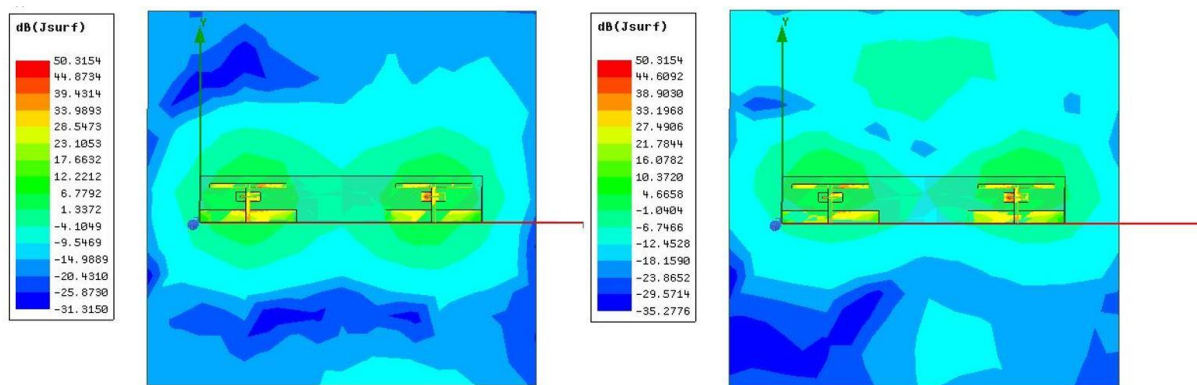


Figure 5.24: The Current Density with Reflector Plate (a) 2.3 GHz (b) 3.5 GHz.

The fabricated antenna is represented in Figure 5.24 and the reflector plate is added to the antenna with a foam due to its light and hollow structure. Scattering parameters are measured and the results are indicated in Figure 5.25. Experimental and simulated data

matches and for 2.3 GHz no losses, however for 3.5 GHz, little mismatch has occurred. For resonans type antenas, mismatch occurs easily but the harmony between the data and simulation should be preserved.

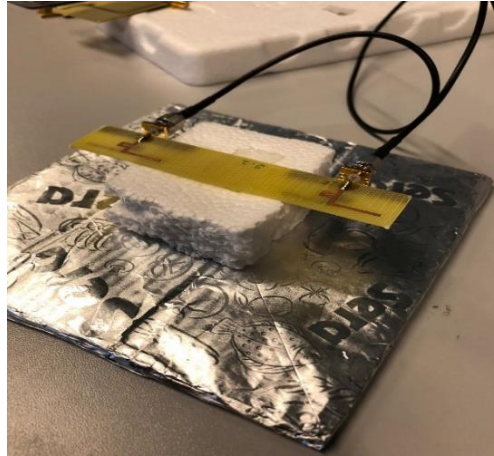


Figure 5.25: Fabricated Antenna.

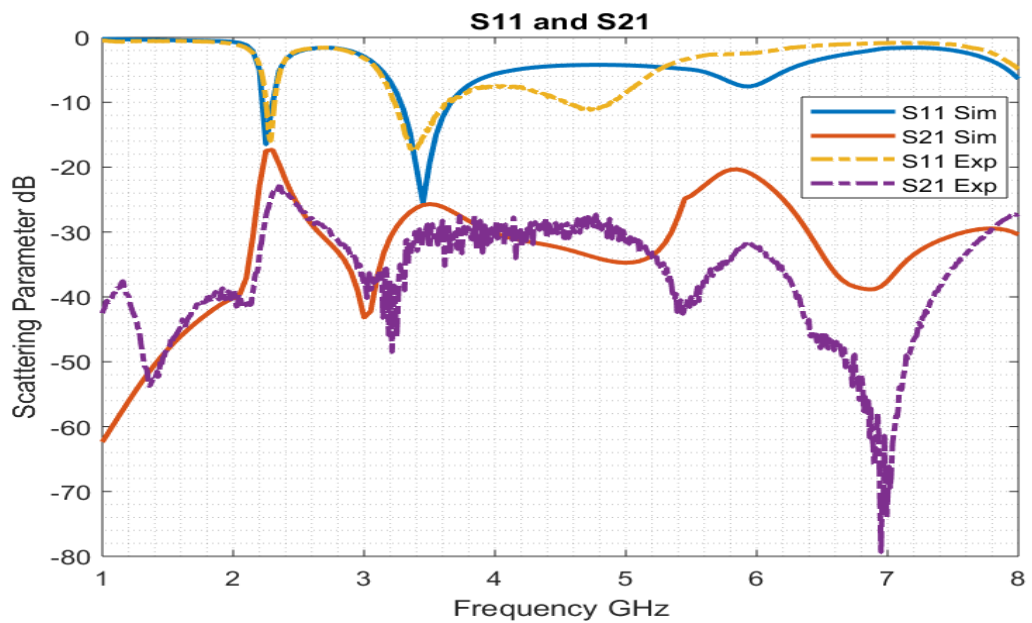


Figure 5.26: S_{11} and S_{12} Graph.



6. CIRCULAR DIPOLE ANTENNA

Wideband antennas are used commonly in communication systems due to their capability for high data transfer and the wide frequency range they include. In this thesis, the reference antenna [14] is optimized to FR-4 substrate because of its easy access and fabrication process. Frequency range is adopted to cover 3.5 GHz and 5.8 GHz and the bandwidth excluded 4.9 GHz and 5.2 GHz. In the design, there are two circles with different radius and the radiation characteristics are realized based on this two geometry. Matching parameters are optimized and simulated by using HFSS. The simulated antenna is fabricated and measured both scattering parameter and far-field radiation pattern. The results are represented in following chapters. After the unit cell design, two element array with two input is simulated. In simulations, the scattering parameter does not shift, however, the sidelobes minimizing is not easy to apply because the antenna operates in wideband. The distance between two element is studied parameterically and for optimized value the antenna is fabricated. The aim is not only having minimum sidelobe and better matching ratio but also the size of the antenna is very important property that should be considered.

6.1 Single Element Design

The single element design is performed by considering the design in [14] and it is adopted to FR-4 by adjusting the frequency range. The simulated antenna is represented in Figure 6.1 and the parameters of the simulated antenna is shown in the Table 6.1. The antenna is fabricated and the results are verified by comparing the experimental and simulated data for unit cell.

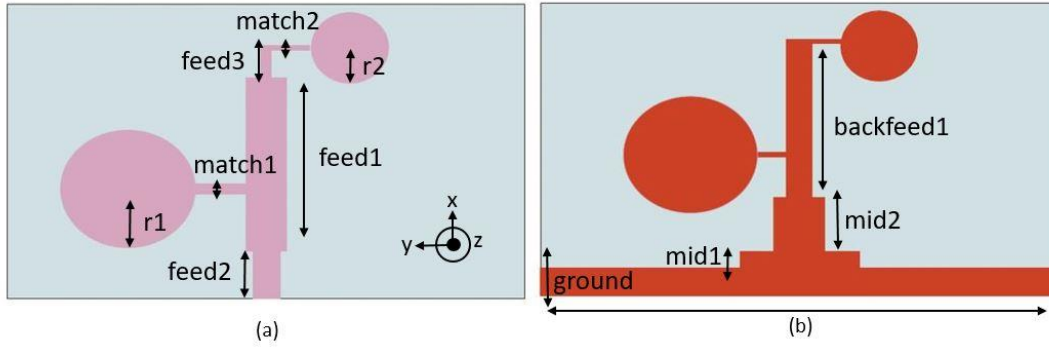


Figure 6.1: Design Configurations of the Antenna a) Front b) Back Side.

Table 6.1: Design Parameters.

Parameter Name	Length on Y direction	Length on X direction	Parameter Name	Length on X direction	Length on Y direction
Match1	4 mm	0.5mm	Match2	1 mm	3 mm
Feed1	4.25 mm	25.5 mm	Feed3	3 mm	0.6 mm
ground	70 mm	4 mm	Mid2	1.75 mm	10 mm
Feed2	2.75 mm	6 mm	Mid1	1.25 mm	12.5 mm
r1	10 mm		r2	5 mm	

The fabricated antenna with reference geometry and the modified geometry is shown in Figure 6.2. The fabricated antennas are measured for scattering parameters and radiation patterns.

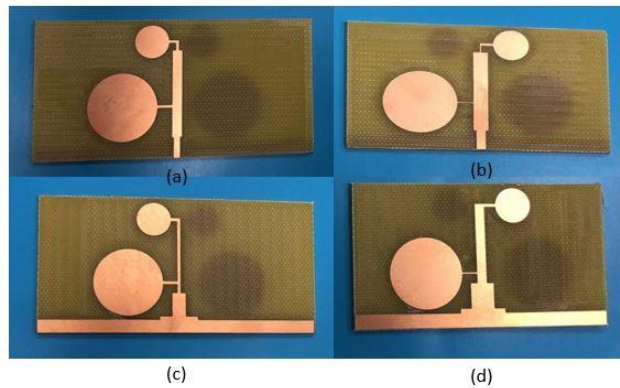


Figure 6.2: Fabricated antennas a),b) Referenced Geometry Ant1[14] c),d) Modified Geometry Ant2.

6.1.1 Simulation and experimental results

The scattering parameter is measured for the fabricated modified antenna and the reference antenna and it is presented in Figure 6.3. As seen in the graph, referenced antenna named Ant1 has the bandwidth between 2.7-4.1 GHz and the resonant frequency is 2.8 GHz in simulation. Beside that, the modified antenna has shifted

spectrum that starts from 3 GHz and ends 6 GHz. The resonant frequencies are 3.3 GHz and 5.8 GHz in interested range.

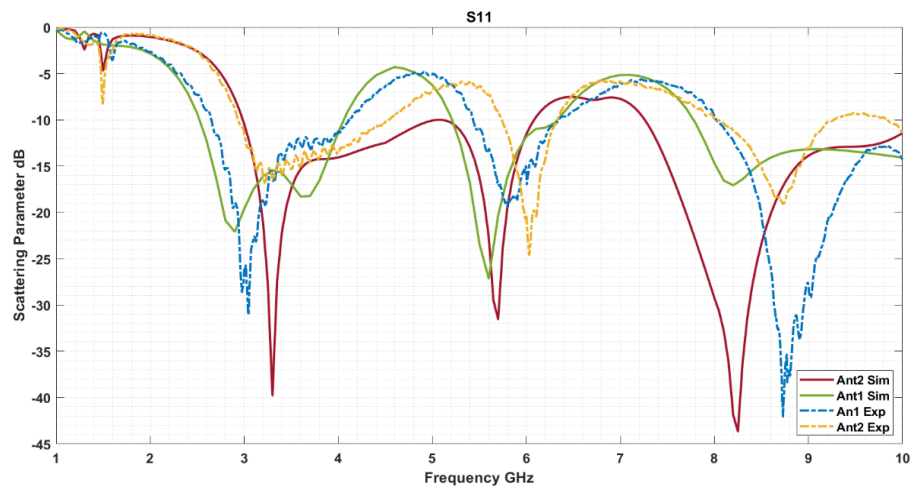


Figure 6.3: S_{11} Result for Reference and Modified Antenna.

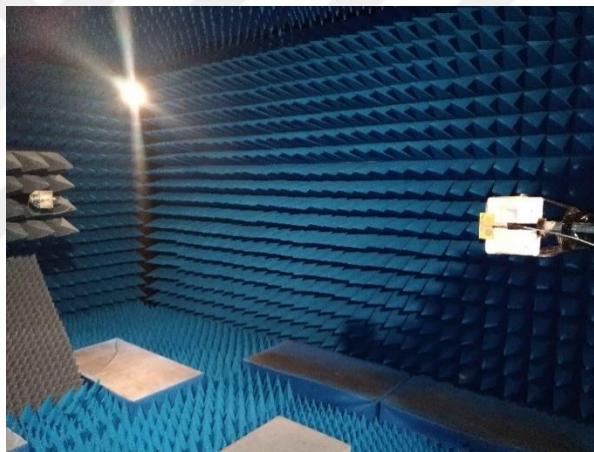


Figure 6.4: Radaiton Pattern Measurement in FarField.

In Figure 6.4, the antenna configuration is shown with the coordinate system it is builded on. The design is performed by using the HFSS and 2D pattern configurations are obtained from this reference coordinate system. In Figure 6.4, the simulated and experimental radiation pattern are drawn and represented. The field patterns are matches with compared to the simulated patterns. For three spesific frequency, which are 3.5 GHz, 4 GHz and 5.8 GHz are considered while realizing the radiation patterns. The simulated maximum gains are 3.5 dB for 3.5 GHz; 3.6 dB for 4 GHz; 3.7 dB for 5.8 GHz.

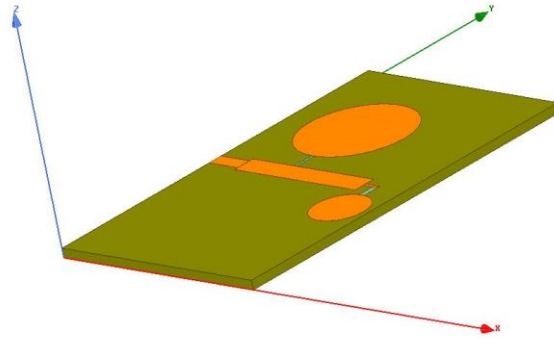


Figure 6.5: Antenna Configuration in Simulation Tool.

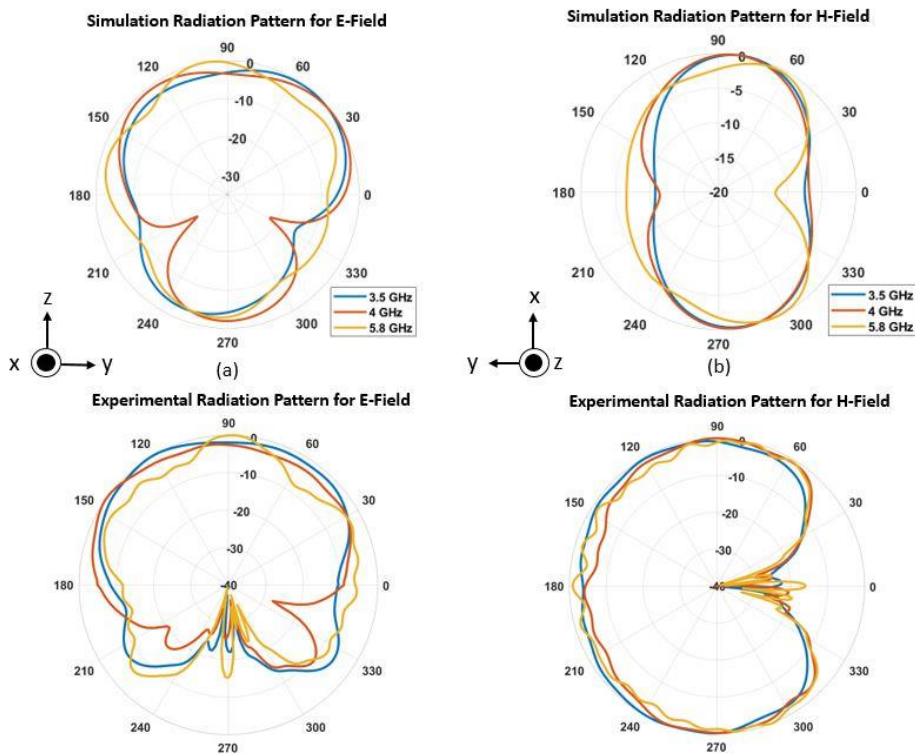


Figure 6.6: 2D Radiation Pattern a),b) Simulated Results; c),d) Experimental Results.

6.2 Two Element Array Design

The modified unit cell circular dipole antenna is designed as an array with two elements and two inputs. The distance between the elements is performed parametrical study which is done by using the HFSS. The distance is determined as 97.25 mm from the ending point of element1 and starting point element 2. This distance requires to adjust the distance between ground planes which is studied as 30 mm. The directivity is increased in this adaptive design and the gain is also increased as a result of it. In

Figure 6.7, the antenna configuration is given by showing the distance parameter. The fabricated antenna is presented in Figure 6.8.

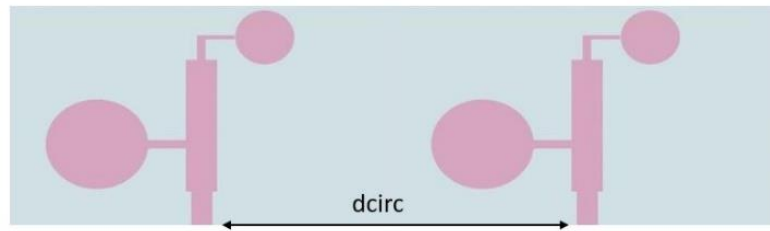


Figure 6.7: Antenna Configuration.



Figure 6.8: Fabricated Antenna.

6.2.1 Simulation and experimental results

The antenna design has two input and as a result of that the S_{11} and S_{21} parameters should be analyzed at the same time. As seen in the Figure 6.9, the S_{21} values do not exceed the -20 dB for both simulated and experimental measurements which is desirable for two input systems. Measured S_{11} values seem coherently with the simulated data. However, experimental data shifts upside compared to the simulated data. Due to the antenna has wideband feature, the radiation patterns are given together in the Figure 6.10 for the frequencies 3.5 GHz, 4 GHz, 5.8 GHz. The simulated gains are 6.0 dB for 3.5 GHz; 6.2 dB for 4 GHz; 6.3 dB for 5.8 GHz which are increased values with respect to the unit cell design.

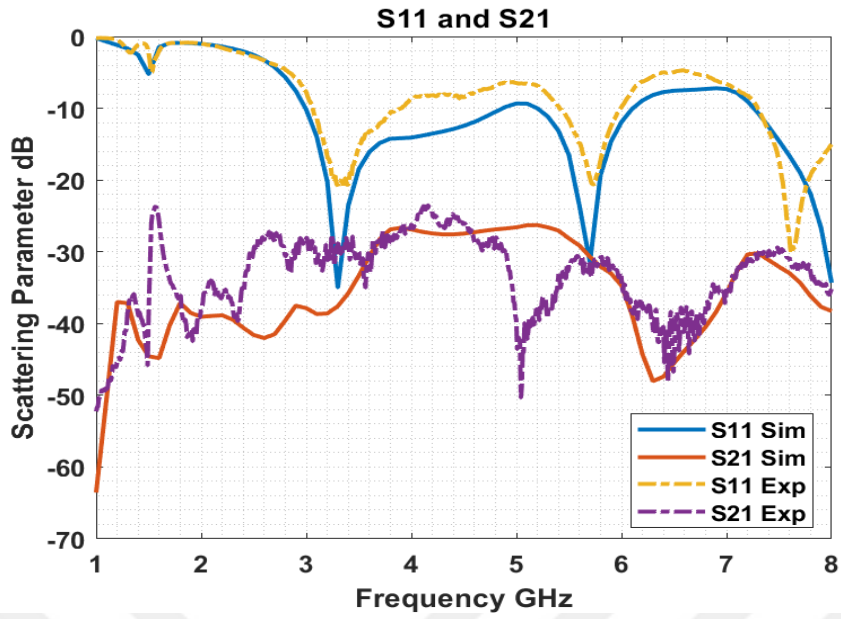


Figure 6.9: S_{11} and S_{21} Parameters.

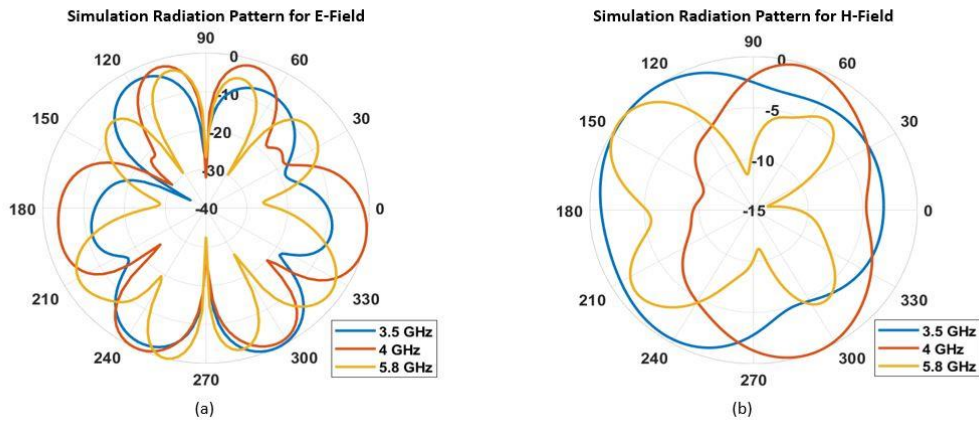


Figure 6.10: 2D Radiation Patterns a) in E-field b) in H-field.

7. K BAND ANTENNA DESIGN

The antenna has been designed to cover off the planing band for 5G mobile communication which includes the operating frequency 28 GHz. A single element simulation is performed by using the CST program to optimize the radiation pattern properties and operation bandwidth. Due to the antenna has a very small size it is a good candidate for array design with many numbers of elements. The small wavelength of 28 GHz, which is almost 10 mm, has a vulnerable nature that can be affected by the outside environment. As a result of this, the antenna has been also simulated with an SMA connector because of its conductive material has effects on the antenna.

7.1 Single Element Design

The unit cell K band antenna has total dimension 20mmx20mm and radiating part $50mm^2$. Feedline is supported by using the coplanar waveguide structure (CPW) on the left and right side. The dielectric material RT/duroid 6035HTC is used in the design, has the properties given in the Table 3.1. On the second design, a reflected element has been added to the antenna structure for that the radiation accumulated in the desired direction. In Figure 7.1, the designed antennas are proposed for two cases. The values of parameters are shown in the Table 7.1.

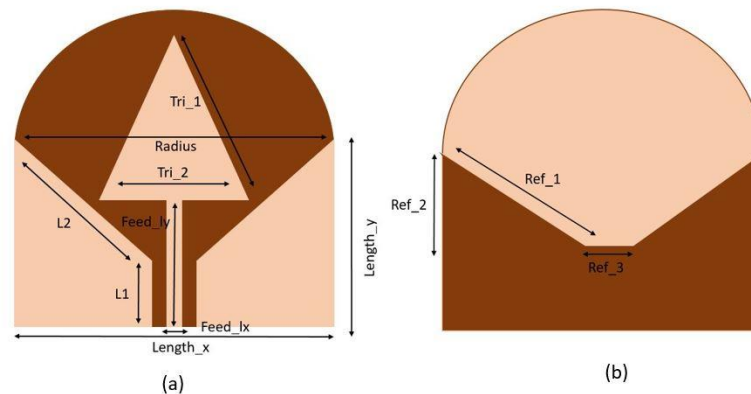


Figure 7.1: Antenna Design a) Antenna without Reflected Back b) with Reflected Back.

Table 7.1: Design Parameters.

Parameter Name	Length	Parameter Name	Length
Length_x	20 mm	Radius	10 mm
L1	5 mm	Length_y	10 mm
L2	10.3 mm	Tri_1	11.18mm
Feed_ly	8 mm	Feed_lx	1.5 mm
Ref_1	10.3 mm	Ref_2	5 mm
Ref_3	2 mm	Tri_2	10 mm

7.1.1 Simulation and experimental results

The antenna has been designed for the purpose of using in array design. Therefore, the size should be minimized by considering the gain and matching factors. In Figure 7.2, antenna drawing in CST program is shown. The antenna has been excited by using the waveguide port feature that CST introduced. CPW is used in case of located a ground plane on backside of the antenna. The antenna operates in bandwidth between 27-32 GHz. The scattering parameter S11 versus frequency graph can be seen in the Figure 7.7.

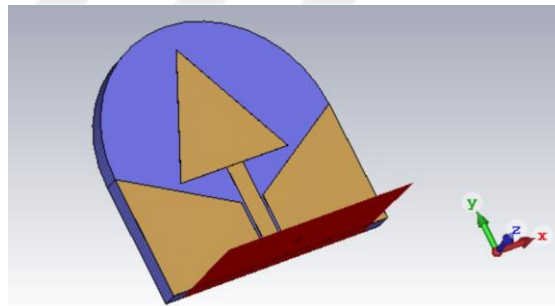


Figure 7.2: Antenna Design Simulation.

In Figure 7.3, simulated far-field radiation patterns are reported for 26 GHz, 28 GHz and 30 GHz. The sidelobes are increased as the frequency is rising. While performing the designed antenna in an array structure requires that minimizing the sidelobes for better-qualified radiation characteristics.

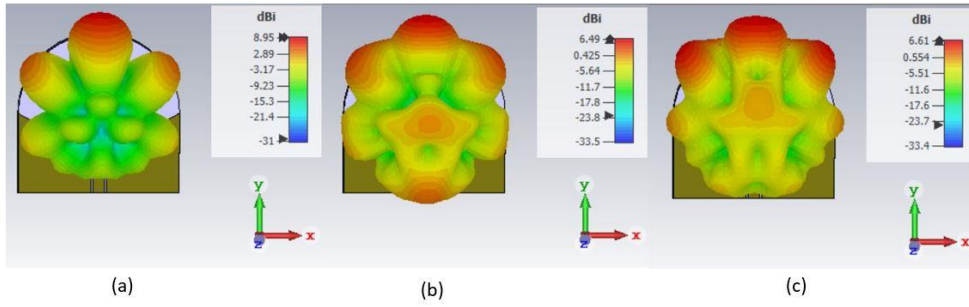


Figure 7.3: Far-Field Gain Results a) 26 GHz, b) 28 GHz, c) 30 GHz.

Besides the purifying the sidelobes in array design, adding a reflector backside of the antenna is also increased the radiation qualification. As seen in Figure 7.4, the radiation patterns for specified frequencies are more directive and side lobes are decreased. However, this reflecting element brings new requirements for matching parameters that should be studied in a process.

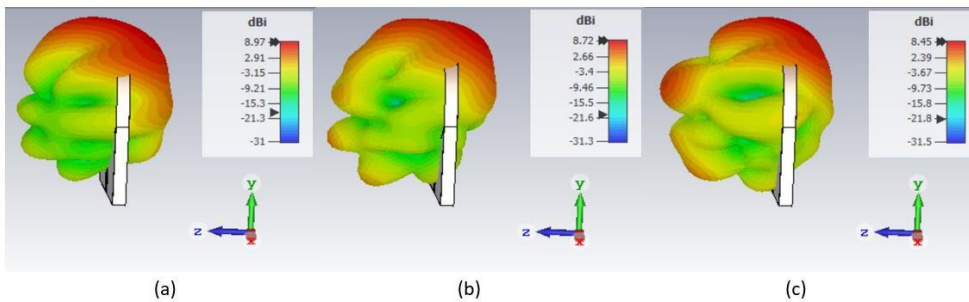


Figure 7.4: Far-Field Gain Results with Reflected Element a) 26 GHz, b)28 GHz, c)30 GHz.

High frequency designs can be easily affected by the outside disturbance. Thus, the designed antenna should be simulated by adding the SMA connector which has the size near to the size of the antenna. The connector has effects directly on the matching which can be seen in the Figure 7.7 that contains the scattering parameters. The far-field radiation pattern for corresponding design is also presented in Figure 7.6.

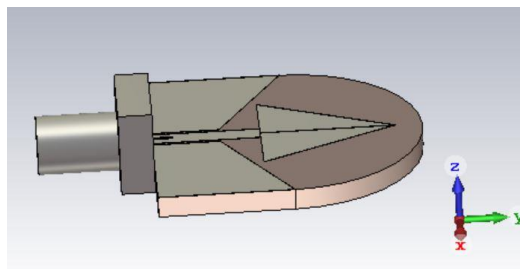


Figure 7.5: Antenna Design with SMA Connector Simulation.

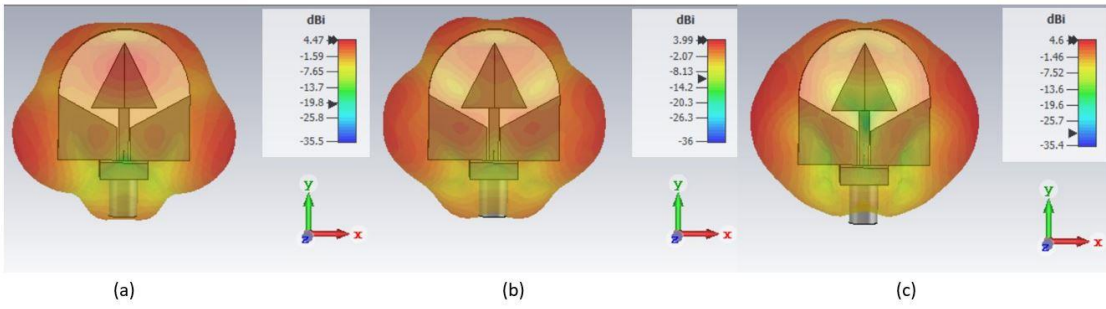


Figure 7.6: Far-Field Gain Results a) 26 GHz, b)28 GHz, c)30 GHz.

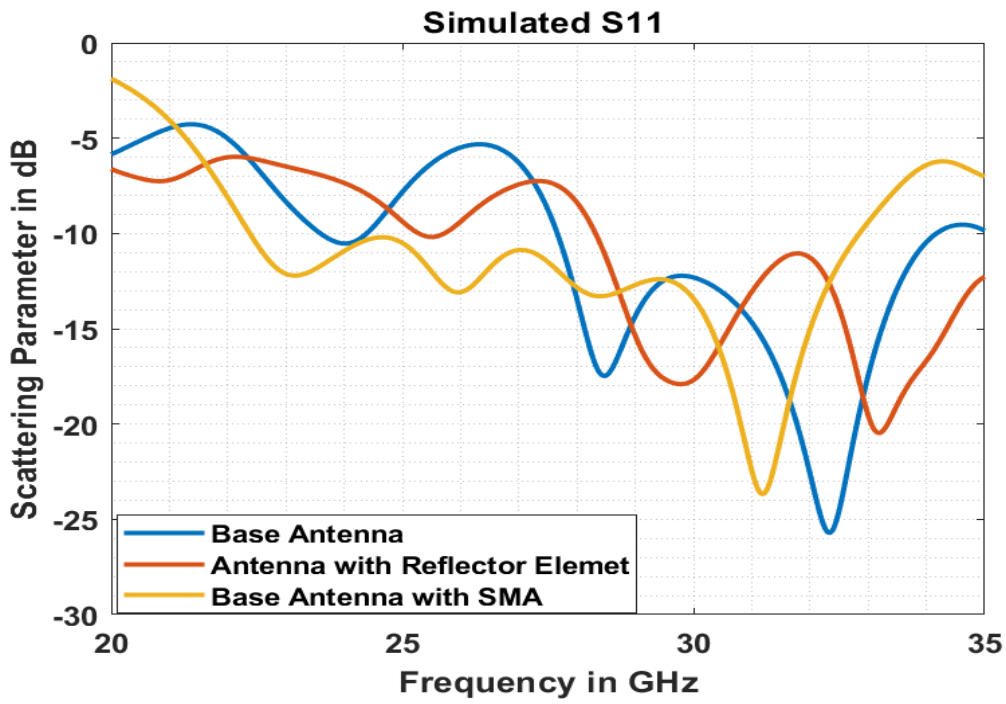


Figure 7.7: Simulated S_{11} Parameters.

8. CONCLUSION AND FUTURE WORK

Various antenna designs have been studied in the thesis by considering the needs that 5G technology will demand. First design is a dual-band Quasi-Yagi type antenna which operation frequencies cover the 2.4 GHz Wi-fi band and 3.5 GHz mobile communication band. The operation bandwidths are narrow bands that can be used for the indoor and outdoor network applications. The unit cell antenna has been studied by performing two element two input array design to enhance the antennas radiation and matching properties. Four element two input array design has been adopted by using a power divider part. However, the gain properties have been increased, the matching parameters of four element antenna succeed on 3.5 GHz. Besides that, in experimental results, its dual-band feature can be observed.

Circular dipole antenna has been designed by adopting the reference design to operate in wideband which covers the 3.5 GHz and 5.8 GHz bands. The antenna has been measured for both matching and radiation pattern properties. After achieving the expected parameters for unit cell, the antenna has been adopted to two element two input array design. Its gain and directivity properties have been increased by performing the design as an array.

The final design is a millimeter-wave antenna which operates at the K_a band with CPW-fed and without a ground plane. Then, the design has been simulated by adding the SMA connector to observe the fluctuations created by the connector. A reflector element has been set on the backside of the antenna due to collect the side radiations.

The antennas designed on FR-4 substrate have been fabricated and measured by using Network Analyzer and the radiation patterns have been performed in anechoic chamber. The K_a band antenna has been simulated and its fabrication process in on the plan. As future work, the K_a band antenna will be designed as an array to study beamforming and multiple inputs and multiple output networks.



REFERENCES

- [1] Cisco Systems Inc., San Jose, CA, USA, “Cisco Visual Networking Index: Global Mobile Data Traffic Forecast Update, 2014–2019,” Available: http://www.cisco.com/c/en/us/solutions/collateral/service-provider/ip-ngn-ip-next-generation-network/white_paper_c11-481360.pdf. Accessed: Apr. 23, 2015.
- [2] Kemp, S. (2019, January 30). Digital 2019: Global Digital Overview - DataReportal – Global Digital Insights. Retrieved from <https://datareportal.com/reports/digital-2019-global-digital-overview>
- [3] GSMA. (2016). 5G Spectrum. *Public Policy Position*, (July). Retrieved from <https://www.gsma.com/spectrum/wp-content/uploads/2016/06/GSMA-5G-Spectrum-PPP.pdf>
- [4] T. Jones and C. Dewing, *Future agenda: the world in 2020*. Oxford: Infinite Ideas Limited, 2011.
- [5] “Spectrum for 4G and 5G,” Qualcomm, 22-Jan-2018. [Online]. Available: <https://www.qualcomm.com/documents/spectrum-4g-and-5g>.
- [6] M. Hermann, T. Pentek, and B. Otto, “Design Principles for Industrie 4.0 Scenarios,” 2016 49th Hawaii International Conference on System Sciences (HICSS), 2016
- [7] Sun, H., Guo, Y. X., He, M., & Zhong, Z. (2013). A dual-band rectenna using broadband yagi antenna array for ambient rf power harvesting. *IEEE Antennas and Wireless Propagation Letters*, 12, 918–921. <https://doi.org/10.1109/LAWP.2013.2272873>
- [8] Lu, W. J., Zhang, W. H., Tong, K. F., & Zhu, H. B. (2014). Planar wideband loop-dipole composite antenna. *IEEE Transactions on Antennas and Propagation*, 62(4), 2275–2279. <https://doi.org/10.1109/TAP.2014.2299820>
- [9] Cheong, P., Wu, K., Choi, W. W., & Tam, K. W. (2014). Yagi-uda antenna for multiband radar applications. *IEEE Antennas and Wireless Propagation Letters*, 13, 1065–1068. <https://doi.org/10.1109/LAWP.2014.2328991>
- [10] Lu, W. J., Zhang, W. H., Tong, K. F., & Zhu, H. B. (2014). Planar wideband loop-dipole composite antenna. *IEEE Transactions on Antennas and Propagation*, 62(4), 2275–2279. <https://doi.org/10.1109/TAP.2014.2299820>
- [11] Sarkar, D., & Srivastava, K. V. (2017). Compact dual-band dual-mode microstrip-fed dipole-loop antennas for pattern diversity arrays. *Electronics Letters*, 53(10), 639–640. <https://doi.org/10.1049/el.2017.0593>
- [12] Çelik, F. T. (2018). Dual – Band Microtrip Quasi – Yagi Antenna Design for Free Band and 5G Mobile Communication, (1), 1–4.
- [13] Eldek, A. A., Elsherbeni, A. Z., & Smith, C. E. (2005). Wide-band modified printed bow-tie antenna with single and dual polarization for C- and X-band

- applications. *IEEE Transactions on Antennas and Propagation*, 53(9), 3067–3072. <https://doi.org/10.1109/TAP.2005.851870>
- [14] El Sayed Ahmad, A., & Floc’H, J. M. (2013). Ultra-wideband quasi-Yagi circular dipole antenna for wireless applications. *2013 Loughborough Antennas and Propagation Conference, LAPC 2013*, (November), 198–201. <https://doi.org/10.1109/LAPC.2013.6711882>
- [15] Wang, B., Zhang, F., Li, T., Li, Q., & Ren, J. (2015). A novel wideband circular patch antenna for wireless communication. *ISAP 2014 - 2014 International Symposium on Antennas and Propagation, Conference Proceedings, 1(mm)*, 545–546. <https://doi.org/10.1109/ISANP.2014.7026767>
<https://doi.org/10.1109/lawp.2019.2940032>
- [16] Liu, S., Wu, W., & Fang, D. G. (2016). Wideband monopole-like radiation pattern circular patch antenna with high gain and low cross-polarization. *IEEE Transactions on Antennas and Propagation*, 64(5), 2042–2045. <https://doi.org/10.1109/TAP.2016.2536418>
- [17] Wong, K.-L., Chou, C.-M., Yang, Y.-J., & Wang, K.-Y. (2019). Multipolarized Wideband Circular Patch Antenna for Fifth-Generation Multi-Input–Multi-Output Access-Point Application. *IEEE Antennas and Wireless Propagation Letters*, 18(10), 2184–2188.
- [18] Li, G., Zhai, H., Li, T., Li, L., & Liang, C. (2013). CPW-fed S-shaped slot antenna for broadband circular polarization. *IEEE Antennas and Wireless Propagation Letters*, 12, 619–622. <https://doi.org/10.1109/LAWP.2013.2261652>
- [19] Lu, Y. J., Liu, Y. W., & Hsu, P. (2014). A Hybrid Design of Printed Antenna Fed by Coplanar Waveguide with and Without Back Conductor. *IEEE Antennas and Wireless Propagation Letters*, 13, 1597–1600. <https://doi.org/10.1109/LAWP.2014.2347348>
- [20] Hua, D., Qi, S. S., Wu, W., & Fang, D. G. (2016). CPW-Fed Printed Antenna Array With Conical Beam. *IEEE Transactions on Antennas and Propagation*, 64(3), 1096–1100. <https://doi.org/10.1109/TAP.2015.2513087>
- [21] Johari, S., Jalil, M. A., Ibrahim, S. I., Mohammad, M. N., & Hassan, N. (2018). 28 GHz Microstrip Patch Antennas for Future 5G. *Journal of Engineering and Science Research*, 2(4), 1–6. <https://doi.org/10.26666/rmp.jesr.2018.4.1>
- [22] Yoon, N., & Seo, C. (2017). A 28-GHz Wideband 2×2 U-slot patch array antenna. *Journal of Electromagnetic Engineering and Science*, 17(3), 133–137. <https://doi.org/10.5515/JKIEES.2017.17.3.133>
- [23] Stutzman, W. L., & Thiele, G. A. (2013). *Antenna theory and design*. Hoboken, NJ: Wiley.
- [24] Balanis, C.A. (n.d.). *Antenna Theory – Analysis and Design (3rd Edition)*. John Wiley & Sons.
- [25] Scattering parameters. (2019, October 4). Retrieved from https://en.wikipedia.org/wiki/Scattering_parameters.
- [26] Welcome to EM Talk. (n.d.). Retrieved from <https://www.emtalk.com/>

- [27] ANSYS Inc. (2019, October 8). hfss-capabilities. Retrieved November 14, 2019, from <https://www.ansys.com/products/electronics/ansys-hfss/hfss-capabilities#cap1>
- [28] ANSYS HFSS: Solve RF Interference Issues. (n.d.). Retrieved from <https://www.ansys.com/products/electronics/ansys-hfss/hfss-capabilities#cap1>
- [29] CST Studio Suite 3D EM simulation and analysis software. (n.d.). Retrieved November 14, 2019, from <https://www.3ds.com/products-services/simulia/products/cst-studio-suite/>







CURRICULUM VITAE

Name Surname : Ferda Cansu GÜL

Place and Date of Birth : İstanbul, 08.06.1992

E-Mail : dede@itu.edu.tr

EDUCATION

- **Bachelor Degree** : 2016, Istanbul Technical University, Science and Letter Faculty, Physics Engineering

WORK

- **Research Assistant** : Istanbul Technical University, Applied Informatics